Master's thesis

NTNU
Norwegian University of Science and Technology
Faculty of Engineering
Department of Energy and Process Engineering

Ronan Njøs Dunne

Investigation of rate capacity retention and mass transport properties of structured cathodes in lithium-ion batteries

Master's thesis in Energy and Environmental Engineering
Supervisor: Odne Stokke Burheim
Co-supervisor: Ejikeme Raphael Ezeigwe and Simon Birger Byremo Solberg
July 2024

NTNU
Norwegian University of Science and Technology

Ronan Njøs Dunne

Investigation of rate capacity retention and mass transport properties of structured cathodes in lithium-ion batteries

Master's thesis in Energy and Environmental Engineering
Supervisor: Odne Stokke Burheim
Co-supervisor: Ejikeme Raphael Ezeigwe and Simon Birger Byremo Solberg
July 2024

Norwegian University of Science and Technology
Faculty of Engineering
Department of Energy and Process Engineering

NTNU
Norwegian University of
Science and Technology

PREFACE

This thesis is written to fulfill the requirements for the author's Master's degree in Energy and Environment (MIENERG), and is completed as part of *TEP4906 Sustainable Energy Systems, Master thesis*, for the Department of Energy and Process Engineering (EPT) at the Norwegian University of Science and Technology (NTNU). This thesis builds upon a project report [1] in *TEP4521 Sustainable Energy Systems Specialisation Project* written by the author of this thesis, however all the experimental work was developed and performed during the spring of 2024 by the author.

I would like to extend my sincerest gratitude to my supervisor, Professor Odne Stokke Burheim for his invaluable help, support and guidance throughout this thesis. Additionally, I would also like to extend my sincerest gratitude to Post-doctoral fellow Ejikeme Raphael Ezeigwe for his great support in the laboratory and for his guidance during the thesis. I am likewise incredibly grateful for all the help and support provided by Ph.D. Candidate Simon Birger Byremo Solberg. I would like to thank NTNU Nanolab for providing the training and use of their Scanning Electron Microscopy equipment.

On a personal level, I am deeply grateful for the support from my family and friends. I could not have completed this undertaking without their unflinching support. Their continual motivation did wonders for my own motivation and willingness to keep going through the tough times.

Ronan Njøs Dunne
Trondheim, July 8, 2024

ABSTRACT

Lithium-ion batteries are increasing in importance as the demand for energy grows during the green transition. Understanding the limitations of batteries in regard to specific energy density and how to overcome them through structural design opportunities could be crucial. This thesis focuses on this understanding by investigating the possibility of increasing specific energy density of lithium-ion batteries by evaluating the relationship between rate capacity retention and mass transport in electrodes. Establishing a robust method for calculating the effective mass transfer coefficient would allow for renewed design of electrodes by maximising use of active material through corrugations in thick electrodes.

This was done by producing electrodes using lithium nickel manganese cobalt oxide, NMC111, as the active material with lignin as a sustainable option for the binder and water as the solvent. The electrodes also contained carbon black as a conductive additive. During the production process of the electrodes, a portion of them were perforated using different mechanical tools to observe the effects of structuring on the mass transport properties and rate capacity retention during characterisation. The structuring was performed on the surface of the electrodes during the production process. Additionally, there were two different thicknesses for the electrodes, 100 and 150 μm, to observe the relationship between electrode thickness and structuring on the results. Before the electrodes were assembled into cells for testing, they were inspected using Scanning Electron Microscopy (SEM) to ensure corrugations were present.

The electrodes were then assembled into coin cells and as part of a three electrode setup containing a gold wire reference electrode (GWRE). The assembled cells were tested using galvanostatic cycling methods to evaluate the electrochemical performance. The rate performance and effective mass transfer coefficient, h_m, were the most interesting aspects of the results. The results were used to plot relative discharge capacity against C-rate to obtain rate capacity retention differences between the structured electrodes and the unstructured ones, including comparing the different thicknesses. The overpotentials were separated into their main component parts (ohmic, reaction and concentration overpotential) to be able to determine the effective mass transfer coefficient at different states of charge (50%,

70% and 90% SoC). This was done by calculating the ohmic resistance to obtain reaction and concentration overpotentials. These were then used to plot Tafel and Butler-Volmer behaviour for the non-ohmic overpotentials to determine that the non-ohmic overpotentials were not due to charge transfer overpotential but rather concentration overpotential. Then the effective mass transfer coefficient could be found and was plotted at various states of charge for the different types of electrode.

The results of the rate capacity retention analysis showed a noticeable improvement in rate capacity retention for structured electrodes compared to unstructured electrodes, especially at high C-rates (3.5C to 5C). This was true for both the thinner and thicker electrodes. At medium C-rates (1C to 3C) the thinner structured electrodes showed a slight improvement in rate capacity retention compared to the unstructured ones, whereas the thicker structured electrodes did not show a significant improvement at medium C-rates. A recurring issue with the mechanical structuring was the non-uniformity of some of the corrugations causing fluctuations in results for the structured electrodes. Overall, the thinner electrodes performed better than the thicker electrodes.

The mass transport analysis showed a clear trend between corrugations on the electrode surface and improved mass transport. The structured electrodes had a significantly higher effective mass transfer coefficient compared to the unstructured variants. At 50% and 70% SoC the tests provided consistent results which showed the increase in effective mass transfer coefficients for structured electrodes. However, at 90% SoC the results were less consistent, especially for the thinner electrodes. This was most likely due to the short time elapsed at this SoC and increased noise, as stationary diffusion regions had not yet developed.

Sammendrag

Litium-ion-batterier blir stadig viktigere etter hvert som etterspørselen etter energi vokser under den grønne omstillingen. Forståelse av batterier og sine begrensninger med hensyn til spesifikk energitetthet og hvordan man kan overkomme disse begrensinger gjennom bruk av strukturell design kan være avgjørende. Denne avhandlingen fokuserer på denne forståelsen ved å undersøke muligheten for å øke spesifikk energitetthet i litium-ion-batterier ved å evaluere forholdet mellom kapasiteten ved ulike lade- og utladingshastigheter og massetransport i elektrodene. Å etablere en robust metode for å beregne den effektive massetransportkoeffisienten vil gjøre det mulig å lage bedre elektroder ved å maksimere bruken av aktivt materiale gjennom korrugeringer i tykke elektroder.

Dette ble gjort ved å produsere elektroder ved bruk av litium-nikkel-mangan-koboltoksid, NMC111, som det aktive materialet med lignin som et bærekraftig alternativ for bindemiddelet og vann som løsemiddel. Elektrodene inneholdt også svart karbon som en ledende tilsetning. Under produksjonsprosessen av elektrodene ble en del av dem perforert med forskjellige mekaniske verktøy for å observere effektene av strukturering på massetransportegenskapene og kapasiteten. Strukturingen ble utført på overflaten av elektrodene under produksjonsprosessen. I tillegg var det to forskjellige tykkelser på elektrodene, 100 og 150 μm, for å observere forholdet mellom elektrodetykkelse og strukturering på resultatene. Før elektrodene ble satt sammen i celler for testing, ble de inspisert ved bruk av skanningelektronmikroskopi (SEM) for å sikre at korrugeringer var til stede.

Elektrodene ble deretter satt sammen i knappceller og som en del av en treelektrode oppsett som inneholdt en referanseelektrode (GWRE). De sammenstilte cellene ble testet ved bruk av galvanostatisk syklingsmetoder for å evaluere de elektrokjemiske ytelsene. Utladingsytelsen og den effektive massetransportkoeffisienten, h_m, var de mest interessante aspektene ved resultatene. Resultatene ble brukt til å plotte relativ utladningskapasitet mot C-rate for å se kapasitetsforskjeller mellom de strukturerte elektrodene og de ustrukturerte, inkludert sammenligning av de forskjellige tykkelsene. Overpotensialene ble delt opp i sine hovedkomponenter (ohmisk, reaksjon og konsentrasjonsoverpotensial) for å kunne bestemme den effektive massetransportkoeffisienten ved forskjellige ladetilstander (50%, 70% og 90% SoC). Dette ble gjort ved å beregne den ohmiske motstanden for å oppnå reaksjons- og konsentrasjonsoverpotensialer. Disse ble deretter brukt til å plotte Tafel- og Butler-Volmer-oppførsel for de ikke-ohmiske overpotensialene for å bestemme at de ikke-ohmiske overpotensialene ikke skyldtes ladningsoverføringsoverpotensial, men snarere konsentrasjonsoverpotensial. Deretter kunne den effektive massetransportkoeffisienten finnes og ble plottet ved forskjellige ladetilstander for de forskjellige typene elektroder.

Resultatene av analysen av kapasitetsytelsen viste en merkbar forbedring i kapasiteten for strukturerte elektroder sammenlignet med ustrukturerte elektroder, spesielt ved høye C-rater (3,5C til 5C). Dette var tilfelle for både de tynne og tykkere elektrodene. Ved middels C-rater (1C til 3C) viste de tynnere strukturerte elektrodene en liten forbedring i kapasitetytelse sammenlignet med de ustrukturerte, mens de tykkere strukturerte elektrodene ikke viste noen betydelig forbedring ved middels C-rater. Et tilbakevendende problem med den mekaniske strukturingen var ujevnheten i noen av korrugeringene, noe som forårsaket variasjoner i resultatene for de strukturerte elektrodene. Totalt sett presterte de tynnere elektrodene bedre enn de tykkere elektrodene.

Massetransportanalysen viste en klar trend mellom korrugeringer på elektrodeoverflaten og forbedret massetransport. De strukturerte elektrodene hadde en betydelig høyere effektiv massetransportkoeffisient sammenlignet med de ustrukturerte variantene. Ved 50% og 70% SoC ga testene konsistente resultater

som viste økningen i effektive massetransportkoeffisienter for strukturerte elektroder. Ved 90% SoC var resultatene imidlertid mindre konsistente, spesielt for de tynnere elektrodene. Dette var sannsynligvis på grunn av den korte tiden som var gått ved denne SoC og økt støy, ettersom stasjonære diffusjonsregioner enda ikke hadde utviklet seg.

CONTENTS

LIST OF FIGURES

LIST OF TABLES

ACRONYMS AND NOMENCLATURE

Acronyms

- **BEV:** Battery Electric Vehicle
- **C:** Coulomb (unit of electric charge)
- **CCCV:** Constant Current - Constant Voltage
- **CHB:** Cyclohexyl Benzene
- **CMC:** Carboxymethyl Cellulose
- **CV:** Cyclic Voltammetry
- **DMC:** Dimethyl Carbonate
- **EC:** Ethylene Carbonate
- **EIS:** Electrochemical Impedance Spectroscopy
- **EMC:** Ethyl Methyl Carbonate
- **EVs:** Electric Vehicles
- **FEC:** Fluoroethylene Carbonate
- **GHG:** Greenhouse Gas
- **GCD:** Galvanostatic Charge and Discharge
- **ICE:** Internal Combustion Engine
- **kPa:** kilo Pascal
- **LIB:** Lithium-ion Battery
- **LIBs:** Lithium-ion Batteries
- **LCO:** Lithium Cobalt Oxide
- **LFP:** Lithium Iron Phosphate

- **LMO:** Lithium Manganese Oxide
- **NCA:** Lithium Nickel Cobalt Aluminium Oxide
- **NMC:** Lithium Nickel Manganese Cobalt Oxide
- **NMP:** N-Methyl-2-pyrrolidinone
- **PPM:** parts per million
- **P:L ratio:** Powder to Liquid ratio
- **PVDF:** Polyvinylidene Fluoride
- **RPM:** revolutions per minute
- **SEI:** Solid Electrolyte Interface
- **SEM:** Scanning Electron Microscopy
- **SoC:** State of Charge
- **SoH:** State of Health
- **TES:** Three electrode setup
- **VC:** Vinylene Carbonate
- **wt %:** Weight percentage

Nomenclature

Symbol	Description	Units
E_{cell}	Standard cell potential	V
E_{cathode}	Standard reduction potential at the cathode	V
E_{anode}	Standard reduction potential at the anode	V
$E_{\text{half-cell}}$	Half-cell potential	V
R	Gas constant	J/(molK)
T	Temperature	K
n	Number of moles of electrons transferred	-
F	Faraday constant	C/mol
E^{rev}	Reversible potential of a battery	V
r	Specific resistance	$\Omega \cdot \text{m}^2$
j	Current density	A/m^2
$\eta_{c.t.}$	Reaction (charge transfer) overpotential	V
$\eta_{conc.}$	Concentration overpotential	V
$\eta_{\text{activation}}$	Activation (reaction) overpotential	V
i	Current	A
i_0	Exchange current density	A/m^2
α	Symmetry coefficient	-
$\eta_{B.V.}$	Butler-Volmer overpotential	V

η_{Tafel}	Tafel overpotential	V
$\eta_{\text{resistance}}$	Resistance overpotential	V
R_{total}	Total resistance in the circuit	Ω
A	Electrode area	m^2
x	Distance	m
D_{Li}	Diffusion coefficient of lithium	-
c_s	Surface concentration	$\frac{\text{mol}}{\text{m}^3}$
c_b	Bulk concentration of the species	$\frac{\text{mol}}{\text{m}^3}$
h_m	Effective mass transfer coefficient	$\frac{\text{mol}}{\text{m}^2 \cdot \text{s}}$
J	Flux of the species	$\frac{\text{mol}}{\text{m}^2 \cdot \text{s}}$
C_{rate}	C-rate	$\text{h}^{(-1)}$

CHAPTER

ONE

INTRODUCTION

A fundamental challenge for humankind in the 21st Century is transitioning to a sustainable society. In 2015, the United Nations set 17 sustainable development goals [2]. The sustainable development goals are a call to action to all countries and cover the areas that need to be achieved in order to transition to a more prosperous world for everyone. These goals include ending poverty, mitigating climate change and protecting Earth and everyone who lives on it.

A major part of mitigating climate change is addressing greenhouse gas(GHG) emissions. As the global average temperature is set to rise by at least 1.5 °C by 2030 [3], there needs to be drastic change to limit this global warming. The energy, industry, transport, food, agriculture and forestry systems worldwide need to be transformed to limit GHG emissions and move toward net-zero emissions [3]. Low-cost, sustainable energy storage solutions are a crucial component for many of these sectors. The transport sector is especially reliant on viable alternatives to fossil fuel powered energy devices. Lithium-ion batteries (LIBs) present a viable alternative for electric vehicles (EVs) to replace the internal combustion engine (ICE) and thus reduce carbon emissions in the transport sector. Lithium-ion batteries are the storage technology of choice for many sectors and thus there has been a substantial growth in LIB production in the past years [4].

The energy storage sector faces an ever increasing demand to improve the energy density of its products to support the green transition the energy industry is undergoing. Lithium-ion batteries could play a key role in achieving net zero emissions. Specifically, improving specific energy density of Lithium-ion batteries will drastically bolster efforts to meet the growing demand for energy in a sustainable way. Though LIBs have been around for a couple of decades [5] there is much left to do in order to surpass traditional energy storage solutions. One of the priorities in the field of battery technology is improving the energy density of batteries. Im-

proving the energy density and rate capacity of LIBs will ensure that fossil-derived energy sources are outperformed and can be phased out completely [6]. One of the main challenges with improving batteries is that the demand for increasing energy density is continuously increasing, leading to a situation with constantly moving goalposts. Approaching the energy density problem can be done in a variety of ways and numerous different approaches are being researched. Many of the approaches are focused on the electrodes, namely changing active material, changing amount of active material and different constituents, changing electrode thickness and design, investigating manufacturing methods and many more [6]. Of course, these all come with challenges. For example, increasing thickness of electrodes affects rate performance of the battery. Investigating the rate capacity retention and mass transport of electrodes of various thicknesses and designs is a promising avenue for increasing the overall performance of LIBs [6].

1.1 Objective and thesis outline

The main motivation behind this thesis is to investigate the relationship between rate capacity retention and the effective mass transfer coefficient in lithium-ion batteries. To achieve this an electrochemical analysis based of voltage-cycling measurements can be used to obtain an effective mass transfer coefficient. This is done by producing electrodes of various thicknesses and with different types of corrugations. Furthermore, investigating how structured electrodes of different thicknesses affect rate capacity retention and the effective mass transfer coefficient will provide insight into increasing specific energy of LIBs. The thesis also targets the possibility of creating a stable three electrode setup that includes a reference electrode in order to support the mass transport analysis.

Chapter 1 of this thesis introduces the scope of the thesis and the main objectives. Chapter 2 consists of the relevant theoretical background needed to follow the methodology and discussions in this thesis, such as lithium-ion batteries and their components, battery production, electrochemical theory and relevant characterisation techniques. Chapter 3 describes the methodology and experimental work performed to obtain the results. This includes the laboratory setup and equipment, production process, characterisation and calculation of the effective mass transfer coefficient. Chapter 4 covers the results and the resultant discussion of those results. The results include rate capacity retention analysis, mass transport analysis and analysis of the surface of structured electrodes using SEM. Chapter 5 covers the conclusions drawn from the thesis. Lastly, chapter 6 covers the suggested further work that could be undertaken to build on this thesis.

1.1.1 Disclaimer

This Master's thesis builds upon the unpublished project report "Increasing energy density with improved transport properties in lithium-ion batteries" by the

author of this Master's Thesis, Ronan Njøs Dunne. The project report was part of the course *TEP4521 Sustainable Energy Systems Specialisation Project* intended to build the groundwork of this thesis and prepare the author for writing this Master's thesis. As a consequence of this, parts of the introduction, theory and methodology are reproduced from the unpublished report on this project [1]. Nevertheless, this Master's thesis is an individual academic research project, and all the experimental work presented in this thesis was performed by the author during the spring semester of 2024.

CHAPTER

TWO

THEORY

This chapter reviews the theory needed to understand the methodology and results presented in this thesis. This includes fundamental battery and electrochemical theory, in addition to the assembly and working principles of different types of batteries and their internal components. Lastly, relevant characterisation techniques and methods used for analysing results are also described in detail.

2.1 Lithium-ion battery

Lithium-ion batteries are energy storage devices that convert chemical energy to electrical energy. The principle behind lithium-ion batteries is that the conversion from chemical to electrical energy occurs through electrochemical reactions in the battery, which are known as oxidation-reduction (redox) reactions. In a redox reaction, one chemical substance is reduced while another is oxidised. Reduction is the mechanism of a compound gaining electrons and becoming negatively charged as electrons are negatively charged particles. Oxidation is the mechanism of a compound losing electrons and becoming positively charged. During this process, one compound increases its oxidation number and the other compound decreases its oxidation number. An oxidation number is the total number of electrons an atom(or compound) gains or loses allowing it to form a chemical bond with another atom [5].

A lithium-ion battery consists of the following main components: anode current collector, anode active material, separator, electrolyte, cathode current collector, cathode active material and battery tabs, as shown in Figure 2.1.1. The anode is the negative electrode where oxidation occurs during discharge. The cathode

is the positive electrode where reduction occurs during discharge. The separator is a physical membrane that prevents contact between the cathode and anode to prevent internal short-circuits. The electrolyte facilitates the movement of ions in the battery. The battery tabs allow for the battery to connected to a circuit in order to be discharged or charged.

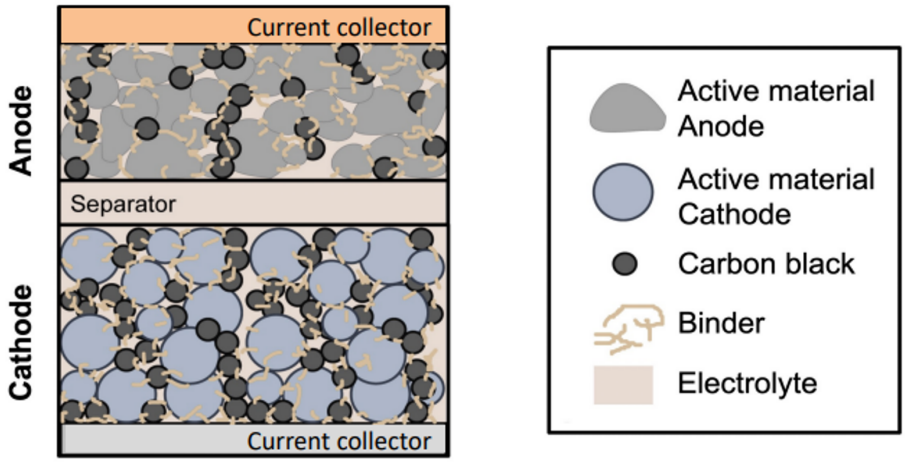

Figure 2.1.1: Schematic of a lithium-ion battery comprised of an anode current collector, anode active material, separator, cathode active material, binder, conductive additive, electrolyte and cathode current collector. Inspired by [7].

The lithium-ion battery structure and components are elaborated on further in subsection 2.1.2. As mentioned earlier, a lithium-ion battery, LIB, operates through a reversible electrochemical process that involves the movement of lithium ions between two electrodes, the anode, and the cathode, which are separated by a separator and doped in electrolyte.

Electrons released during the oxidation of the anode travel through the battery tabs to an external circuit, providing electrical energy to power devices or systems connected to the battery. Simultaneously, lithium ions migrate through the electrolyte from the anode to the cathode. This movement is facilitated by the ionic conductivity of the electrolyte. When the battery is charged, an external voltage is applied, causing lithium ions to move from the cathode back to the anode. As a consequence, electrons are forced to flow in the opposite direction, storing electrical energy in the battery.

This process is reversible and can be repeated through numerous charge and discharge cycles. The ability of lithium ions to move between the anode and cathode while storing and releasing energy forms the basis of the rechargeable nature of lithium-ion batteries. The overall efficiency and performance of the battery depend on the materials used for the electrodes and electrolyte, influencing factors such as energy density, power density, cycle life and ageing [5]. This process is illustrated in Figure 2.1.2.

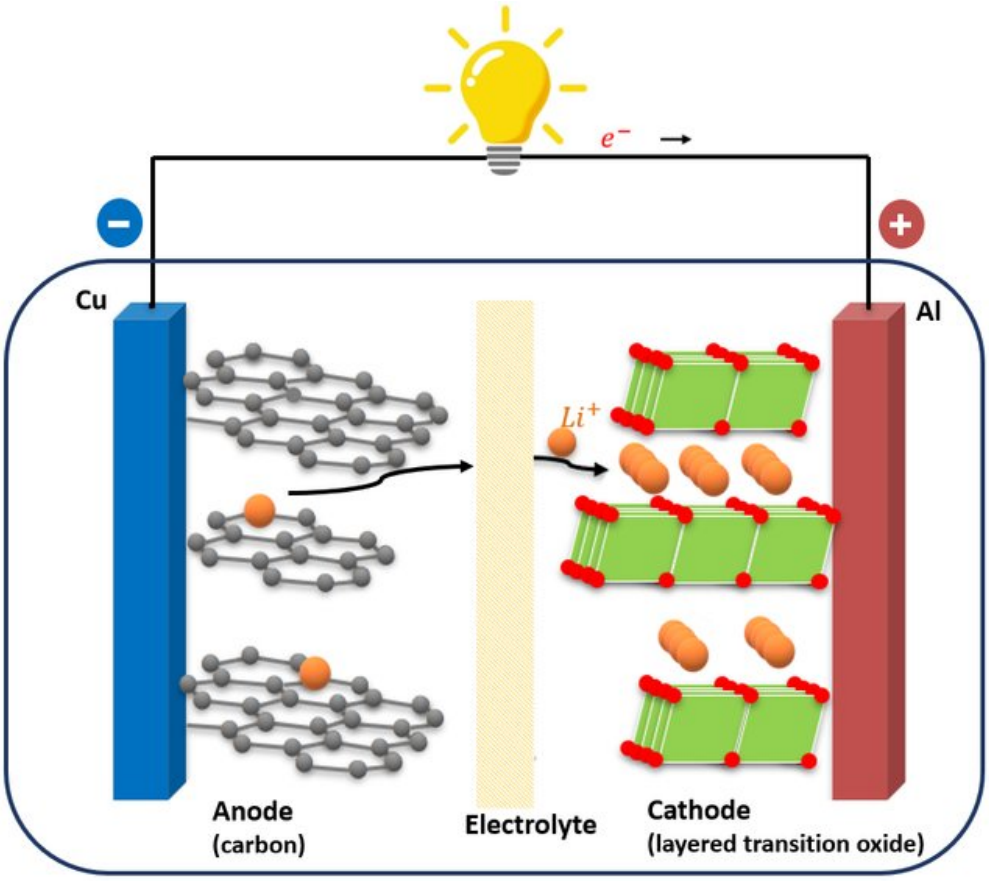

Figure 2.1.2: Schematic of a lithium-ion battery undergoing a discharge process where electrons are transferred from the carbon anode to the cathode through the external circuit while the lithium-ions diffuse through the electrolyte to the cathode. Figure taken from Spitthoff et al. [8].

2.1.1 Battery types

There are many different battery types used and this section will explore some of the more commonly used ones. Lithium-ion batteries come in various types, each tailored to specific applications and requirements. The three most commonly used battery housing types are cylindrical (round), prismatic and pouch cells as shown in Figure 2.1.3.

Cylindrical cells consist of a long rectangular battery rolled up into a cylindrical container with a cover. Cylindrical cells often resemble traditional AA or AAA batteries, are versatile and used in a wide range of consumer electronics. Prismatic cells consist of several battery layers stacked inside a rigid container. Prismatic cells have a flat and rectangular shape and are common in portable electronics and electric vehicles that require a robust packaging system. Pouch cells consist of several battery layers that are stacked inside a plastic bag. Pouch cells are flexible and lightweight, and employed in applications where form factor and weight are critical, such as in mobile devices and electric vehicles [5].

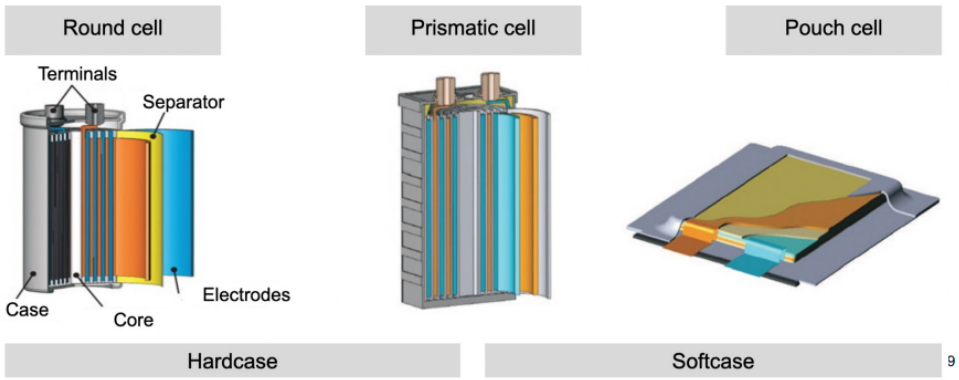

Figure 2.1.3: This is an illustration of a round, prismatic and pouch cell. Figure reproduced from [9].

Choosing the right battery type involves considerations of use case, energy density, power requirements, and cost. The diverse array of LIB types allows for customisation to meet the specific needs of various industries and applications. In Table 2.1.1 the three main battery housing types are compared with their respective advantages and disadvantages.

Coin cells

Coin cells, or button cells, are the smallest type of battery. They are characterised by their compact size and cylindrical shape. Most often used in small electronic devices like watches and hearing aids. The voltage of coin cells varies depending on the chemistry, Lithium coin cells typically have a nominal voltage of 3 volts, while silver oxide cells commonly provide 1.55 volts.

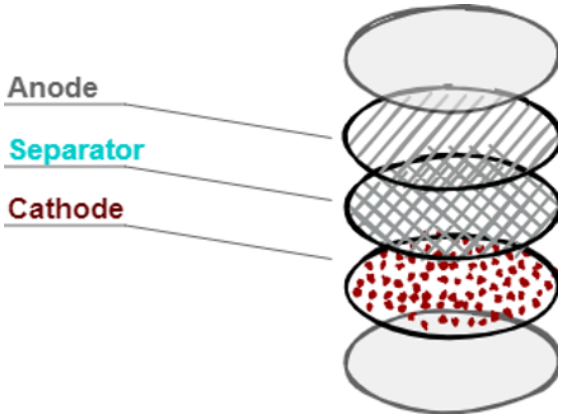

Figure 2.1.4: Simplified illustration of a coin cell.

Table 2.1.1: Comparison of main Battery Housing Types.

Housing Type	**Advantages**	**Disadvantages**	**Capacity range**
Cylindrical (round) cell	• Established format and production process • High volume of production possible	• Bad packaging properties on a module and system level • Irregular temperature distribution • Requires more components for assembly than pouch cells	• 3.1 - 3.9 Ah
Prismatic cell	• Good packaging properties at a module/system level • Good cooling properties compared to round cells	• Depending on the process can have intermittent coating • relatively high weight • Complex housing structure • More components/ production steps	• 20-300 Ah
Pouch cell	• Inexpensive, even for small quantities • Fewer production steps • High energy density • Fewer components -> reduced complexity • Good cooling properties	• Poor mechanical resilience • Poor sealing tightness • low fatigue strength	• 2 - 70 Ah

Three electrode setup

A three electrode setup, TES, isn't a typical type of commercial battery but rather one that is more common in academia and research. A TES consists of a cathode, an anode and a reference electrode. This setup allow the cathode and anode potential contributions to be separated and thus can be analysed to learn about the individual performance of the cathode and anode. An example of when this could be useful is when analysing degradation of specific electrodes [10] or over-potential contributions. During testing of the TES, one electrode (cathode or anode) will be designated the working electrode and the other the counter electrode. The working electrode is the electrode of interest in terms of analysing individual contributions. The reference electrode is stable and does not participate

in the reaction but allows the change in potential to be measured while a current is applied to the working and counter electrode. TES can also be used to measure impedance differences between the electrodes [11–13].

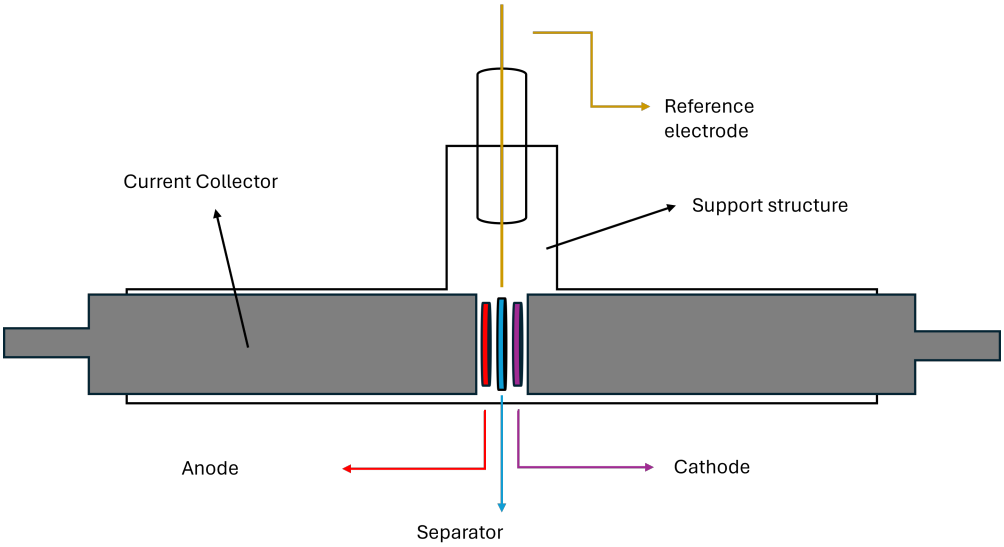

Figure 2.1.5: Illustration of a typical three electrode setup containing anode, cathode and reference electrode.

2.1.2 Electrodes

As mentioned earlier, a lithium-ion battery is made up of two electrodes with different electrode potentials. The positive electrode is also called the cathode. The cathode is made up of a current collector coated with active material. One of the most common commercial batteries is a Lithium cobalt oxide, LCO, battery [14]. The LCO battery consists of a $LiCoO_2$ cathode and a carbon graphite anode. Equation 2.1 and Equation 2.2 show the chemical reactions for the battery occurring at the anode and cathode.

$$Anode : \mathrm{Li}_x\mathrm{C}_6 \rightleftharpoons \mathrm{xLi}^+ + \mathrm{xe}^- + \mathrm{C}_6 \tag{2.1}$$

$$Cathode : \mathrm{Li}_{1-x}\mathrm{CoO}_2 + \mathrm{xLi}^+ + \mathrm{xe}^- \rightleftharpoons \mathrm{LiCoO}_2 \tag{2.2}$$

Cathode

The cathode is composed of lithium cobalt oxide (LiCoO_2) or other lithium transition metal oxides. During discharging, lithium ions from the anode move through

the electrolyte towards the cathode. The cathode active material ranges in size from 90 - 130 μm and the cathode current collector is often below 30 μm.

A LIB cathode consists of the following key ingredients: cathode active material, conductive material, a binder and a cathode current collector. The conductive material is an additive that aids in the electrical conductivity of the active material in the cathode [15].

The most common conductive material in LIBs cathodes is carbon black. The binder is an additive used to improve adhesion of the active material to the current collector. The binder also enables a stronger connection between the conductive additive and active material. This connection can prevent excessive mechanical and chemical stresses from damaging the active material discharge and charging cycles [16].

Polyvinylidene fluoride, PVDF, is the most common binder in use for LIBs due to its tendency to bind solidly to current collectors. PVDF has some drawbacks which can make it a problematic choice. Fluorinated polymers like PVDF can cause decreased cycling performance in batteries due to a reaction with lithium metal which causes formation of stable LiF and double bonds [17]. The reaction between PVDF and Lithium is exothermic (reaction which releases energy), which could cause thermal runaway[18]. Thermal runaway is an effect caused by increasing temperature that can trigger an exothermic reaction that will generate heat faster than the battery can cool down. This sets off a chain reaction of further temperature increase and ultimately leads to a potential explosive reaction [5]. Lastly, PVDF needs to be dissolved in an organic solvent, typically N-methyl-2-pyrrolidinone, NMP, to produce slurry for the coating process. It is important to note that NMP is toxic to both humans and the environment. [19]. All these factors make PVDF a sub-optimal choice in terms of sustainable and renewable production of environmentally-friendly LIBs. Therefore alternative binders are necessary in order to enhance sustainability of LIBs.

Lignin is a by-product from pulp and paper industry that is an attractive alternative to PVDF as a binder. This is because lignin is renewable, cheap and plentiful. Lignin is a promising option for use as a sustainable binder choice in lithium-ion batteries but needs more testing to fully understand the potential adverse effects on LIB performance [19].

There are a few key properties the cathode material of a LIB should have in order to be a suitable candidate for optimising performance of said LIB [20]. These properties are as presented in the following list:
1. High free energy reaction with lithium which leads to a high working voltage.
2. High energy density and recharge-ability.

3. Ability to intercalate Li-ions at a high rate which leads to a high power capability.
4. Ability to incorporate Li-ions without causing structural changes. This is necessary to be enable long cycle life.
5. A high electrical conductivity without reacting with the electrolyte.
6. Relatively low cost and commercially abundant.

In LIB's there are many different types of cathodes each with their own individual chemical makeup. The five most common active materials are Lithium Nickel Manganese Cobalt Oxide (NMC), Lithium Nickel Cobalt Aluminium Oxide (NCA), Lithium Manganese Oxide (LMO), Lithium Iron Phosphate (LFP) and Lithium Cobalt Oxide (LCO). Each of them have their own advantages and disadvantages, with a wide range of applications for all of them. Figure 2.1.6 is included as an graphical representation of these differences [21].

Figure 2.1.6: This is a figure showing the strengths of the main cathode chemistries and compared against each other. Figure taken from Zubi et al.[21]

NMC is a versatile cathode chemistry that is widely used since it has good specific energy and specific power density. It can be set up in different configurations depending on the application of the LIB. Two common configurations are

NMC111 and NMC811. The numbers represent the share of Nickel, Manganese and Cobalt in the cathode material. NMC111 equates to a chemical configuration of $LiNi_{0.33}Mn_{0.33}Co_{0.33}O_2$ and NMC811 equates to a chemical configuration of $LiNi_{0.8}Mn_{0.1}Co_{0.1}O_2$. NMC cathodes can be designed for high specific energy or power with high energy density. Nickel has high specific energy but poor thermal stability whereas Manganese and Cobalt provide chemical and structural stability [22]. NMC811 is a structure designed to have a high specific energy due to its high Nickel content and a reduction in Cobalt lowers the overall cost of the electrode [23]. Common applications for NMC electrodes are battery electric vehicles, BEVs, power tools and grid energy storage. NMC has a layered structure.

NCA is a cathode chemistry that has high specific energy and good life span but has safety issues. It has been around since 1999 but is not as widely used as other more popular configurations such as NMC electrodes. Additionally, even with the relatively low Cobalt content, they are more costly to manufacture than many other chemical configurations [23]. NCA has a layered structure.

LFP is a cathode chemistry with moderate density, great safety and a wide range of operating temperatures (+60 °C to 30 °C). This is because the Phosphate part protects against overcharging and gives the electrode a higher heat tolerance which increases the operating temperature range considerably. Common thermal issues, e.g. thermal runaway, are not as prevalent in LFP electrodes [23]. Due to these features LFP is a versatile cathode chemistry with a wide range of applications ranging from personal transport to auxiliary aviation systems. LFP has an olivine structure.

LMO is a cathode chemistry that has been around since the 1980's with low internal cell resistance due to its spinel structure. This allows for fast charging and high current discharging. Another facet of this chemistry is its increased thermal stability compared with an LCO battery but lower life span and capacity [23]. These features mean LMO electrodes are usually used in LIBs where these properties are acceptable, e.g. mobile phones or laptops.

LCO is a cathode chemistry that is very interesting due to its high theoretical specific capacity, high theoretical volumetric capacity, long life cycle, good cycling performance and ease of manufacture[17] [23] [24]. One of the main issues with this cathode material is the cobalt. Mining of cobalt is associated with unethical practices and has a high cost. Cobalt has low thermal stability which can result in a thermal runaway situation irreversibly damaging the battery [25].

Anode

Anode materials are important in LIBs as they are needed to mitigate the challenges associated with the use of lithium metal. Lithium metal forms dendrites during cycling [24]. These dendrites, needle-like structures that grow from the surface of the lithium electrode, pose significant risks. They can cause internal short circuits within the battery, initiating a thermal runaway reaction on the cathode, and potentially leading to an unusable battery. Moreover, the use of lithium metal as an anode material presents issues related to poor cycle life. Continuous cycling leads to the degradation of the lithium metal, reducing the overall efficiency and longevity of the battery [24].

The anode is typically made of graphite. During the discharging process lithium ions in the anode release electrons and move towards the cathode through the electrolyte. A LIB anode consists of conductive material, a binder, anode active material, anode current collector and additives. The anode structure is comparable to a LIB cathode except that the chemistries are different. The active material ranges from 70 - 100 μm and the current collector is often less than 30 μm.

The most common conductive material in LIB anodes is carbon black. It has the same function as in the cathode where it increases electrical conductivity for the active material. Similarly to cathodes, the most common trace additives added to anodes are: pore-forming agents, wetting additives and safety additives.

Unlike the cathode, where PVDF is commonly used as a binder, the anode often utilizes carboxymethyl cellulose (CMC) as a binder. CMC forms a stable and flexible matrix when combined with the anode's active materials, promoting good adhesion between the conductive additive and the active material. This helps maintain the mechanical integrity of the anode during the battery's operation. Additionally, CMC is known for its compatibility with aqueous solutions, providing a more environmentally friendly alternative to organic solvent-based binders [26].

The anode in LIBs plays a pivotal role in determining the battery's capacity, rate capability, and cycle life. Carbon (graphite) is still the anode material of choice ever since it's introduction in 1991 [27].The appeal of carbon as an anode material lies in its decent characteristics and the relatively low cost, abundant availability, moderate energy density, power density, and cycle life—especially when compared to other anode materials. Notably, carbon's gravimetric capacity exceeds that of most cathode materials. However, limitations like relatively low energy density, volumetric capacity and structural degradation upon cycling have

spurred research into alternative anode materials [28] [24].

Over the years, new anode active materials have emerged. Hard Carbon emerged in 2003 and has a greater storage capacity than graphite and has excellent stability during cycling [29]. One of the primary applications for hard carbon as an anode active material is in home electronics LIBs.

Alloys, such as a Tin-Cobalt alloy were introduced around 2005. The main advantages of alloy based anode active materials are high specific capacity and good security. Some of the main limitations are the relatively low electrical conductivity and large volume increase [29][30].

Transition metal-oxides, such as lithium titanate, LTO, have been around since 2008. LTO has the advantage of being very stable during charge and discharge cycles. The specific capacity is also relatively high. The main limitations are the poor coulombic efficiency [29]. LTO has recently commercialised and has seen use in LIBs used in buses.

Finally, there are other anode materials, such as silicon and silicon-carbon, which offer higher theoretical capacities. Silicon can absorb a larger amount of lithium, significantly increasing the anode's capacity. However, challenges such as volume expansion during lithiation and delithiation cycles must be mitigated to ensure structural stability. Additionally, Silicon is an abundant and inexpensive resource [29].

2.1.3 Electrolyte

The electrolyte is a solution made up of conductive salts, which serves as the conductive medium for lithium ions between the anode and cathode during electrochemical reactions in lithium-ion batteries. The electrolyte enables the movement of ions while preventing the direct flow of electrons, maintaining the overall charge balance. Composed of lithium salts (LiPF6 and LiBOB) dissolved in organic solvents (EC,PC,DMC,EMC), the electrolyte's composition significantly influences the battery performance, safety, and thermal stability. An electrolyte composition consists of a solvent, conductive salt and additives. The different conductive salts, solvents and additives each bring their own advantages.

An example composition could be the following:

1. **Solvent:** 1:1 ratio of Ethylene carbonate (EC): Ethyl methyl carbonate (EMC). EC has a cyclical structure for increasing the boiling temperature. EMC has a

linear structure for improved ion mobility.
2. **Conductive salt:** Lithium hexafluorophosphate (LiPF6) : 1 M.
3. **Additives:** 2 % Vinylene Carbonate (VC), which supports SEI development. 3 % Cyclohexyl benzene (CHB), which provides overcharge protection.

As with most LIB elements, the electrolyte has to meet certain requirements. The most important of these that an electrolyte must satisfy are the following: (1) facilitating the formation of a stable passivating layer; (2) possessing limited volume expansion; (3) having high ionic conductivity; and (4) featuring low flammability [31].

The current leading liquid electrolyte formulation comprises a lithium salt dissolved in a blend of ethylene carbonate (EC) and a linear carbonate like dimethyl carbonate (DMC). This blend not only ensures high conductivity but also fosters favorable electrode passivation, mitigating parasitic side reactions. However, challenges pertaining to the safety of these liquid electrolytes persist, necessitating further advancements to address and overcome these concerns [31].

Researchers focus on optimising electrolyte formulations to meet the requirements for a good electrolyte and enhance ionic conductivity, thermal properties, and electrochemical stability. The choice of electrolyte additives, such as fluoroethylene carbonate (FEC) or vinylene carbonate (VC), is important in forming a stable SEI, reducing impedance, and improving cycle life.

2.1.4 Separator

The separator in lithium-ion batteries is a porous physical, non-conductive (electrically), thin, permeable membrane positioned between the cathode and anode, preventing direct contact between the electrodes and short circuits while facilitating the lithium-ion transfer [5].

There are a vast range of separator materials that can be used. There are nonwoven fibers like cotton, nylon, polyesters and glass. There are polymer fiber like polyethylene, polypropylene and polyvinyl chloride. Then there are naturally occurring materials like rubber, asbestos and wood that could theoretically be used. Polymeric separators, often made of polyethylene or polypropylene, dominate the industry due to their excellent chemical stability and mechanical strength. Separators range in size from 20 - 25 μm.

A separator generally consists of a polymeric membrane. Ideal properties for

a separator are mechanical strength, chemical stability, electrochemical stability, and thermal stability. Other properties that determine whether a membrane is suitable as a separator include high wettability for the electrolyte, good permeability, and high porosity for efficient ion transport [32] [31]. The separator needs to be tailored to the corresponding LIB it will be used in and performance needed. The thickness of the separator must be carefully chosen to strike a balance between its mechanical properties and its ability to facilitate the transport of lithium ions. If the separator is too thin it might not be mechanically strong enough. Additionally, the separator should stop the diffusion of electrode components or cathode products, particularly at higher temperatures [33]. The performance of separators is influenced by their mechanical properties, ionic conductivity, and tortuosity [31].

2.2 Battery production

Lithium ion production is an energy intensive and complex process. One of the most energy intensive parts of LIB production is the manufacturing of electrodes and has a huge impact on LIB performance [34]. Though there are differences in LIB production, e.g. small scale laboratory production versus large scale industrial production, generally the production process is similar but the equipment used might be quite different.

The manufacture of a LIB typically follows the recipe shown in Figure 3.2.2. The production process starts by creating a mixture, or slurry, that includes a binder, an active material, a conductive additive, and a solvent. This slurry is then coated onto a current collector, typically aluminum for cathodes and copper for anodes. Once the slurry has solidified enough to be moved, the solvent is then removed through drying. In a lab this is often done using a vacuum oven, or autoclave. The next step is calendaring the coating to reach specific thickness or density. Calendaring compresses the material. Once the electrode has been calendared to the desired thickness, it is cut into the desired shape. This shape depends on the type of battery it is, e.g. for coin cells the electrode would be cut into small circular electrodes. The cell is then assembled and the electrolyte is introduced in a controlled, low-humidity environment like a dry-room [6].

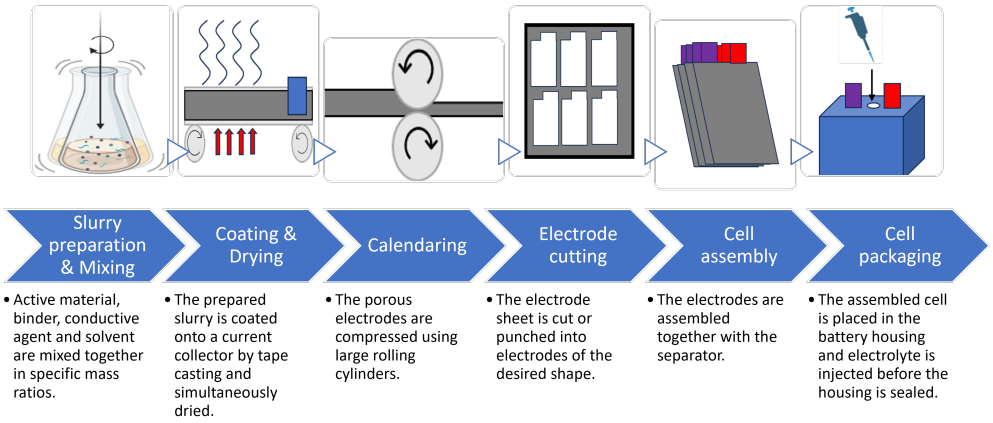

Figure 2.2.1: This is an illustration showing and describing the production process for a lithium-ion battery in a lab. Inspired by [35]

In electrode production, the formulation of electrode materials into slurries and the application of coatings determine the electrochemical performance. Techniques like slurry preparation and coating influence the thickness, porosity, and uniformity of electrodes, impacting the overall efficiency of the battery.

Calendaring is a critical step to compress and improve the mechanical integrity of electrodes, ensuring good electrical contact and enhancing stability during cycling. Electrode cutting techniques, whether dry or wet, influence precision, speed, and potential thermal effects.

Cell assembly involves integrating electrodes, separator, and electrolyte into a finished cell. Techniques for stacking, winding, or folding components vary depending on the battery type. Quality control during assembly is crucial to identify defects and ensure consistent performance across batches.

Advancements in production methods contribute to scaling up manufacturing, reducing costs, and improving the overall quality and reliability of lithium-ion batteries.

2.2.1 Cathode production

As discussed earlier, the cathode is a vital component of lithium-ion batteries, influencing the energy density, voltage, and overall performance. Cathode performance is affected by most steps in the production process. Slurry production,

coating of the current collector, drying and calendaring of the electrode all affect the performance of the finished product [6]. The homogeneity of the slurry and the adhesion and particle cohesion of the dry coated electrode affects the electrode performance through voltage, capacity and impedance variations. The rheology of the slurry and the mechanical strength of the dry coated electrode affect the uniform current density of the electrode. The clustering of carbon black on the slurry and the porosity of the dry coated electrode affects the electrode battery performance through efficiency, power density and energy density variations. The tortuosity of the dry coated electrode affects the safety, the lifetime stability and the cycle stability of the electrode [36–38].

Slurry preparation and mixing

The first step in cathode production is the preparation of the slurry. The slurry preparation begins with considering the composition of active material, binder, conductive additives and solvent to obtain a homogeneous electrode which improves LIB performance as mentioned earlier. A typical ratio for active material,conductive additive and binder could be 90:5:5 [35]. The amount of solvent to to dissolve the electrode components is known as the powder:liquid ratio wt %, P:L. A typical P:L ratio could be 1. These specific mass ratios vary and depend on the desired properties of the slurry.

There are a variety of methods for mixing the active material, conductive material and binder material. Mixing is important to ensure a homogeneous mix with specific porosity for lithium ion diffusion while maintaining electron transport. A common method of mixing is starting with mixing of the dry part and then mixing the dry part with a solvent. This is done to activate the binder, help in reducing clustering and to adjust the viscosity for optimal coating [39]. The duration and intensity of the mixing is important for porosity, adhesion and viscosity. Some common types of dry mixing devices are: (1) rotary drum mixer, (2) Eirich intensive mixer and (3) high energy mixing device. A rotary drum mixing is used for distributive dry-mixing. An eirich intensive mixer is used for intensive dry mixing. A high energy mixing device is used for high intensive dry-mixing. An extrusion process is a continuous mixing and dispersion process used on an industrial scale to improve ability to reproduce the slurry mixture [6].

Coating and drying

The next step in the production process is the coating of electrode slurry onto a current collector and subsequent drying of the electrode.The coating and drying is often performed continuously on long process lines so the process starts with a clean current collector and ends with a dried electrode ready for calendaring.

There are two main types of industrial coating units, comma-bar and slot-die as shown in Figure 2.2.3a and Figure 2.2.3b with some key properties described in Table 2.2.1 [39]. A typical lab coating unit is a vacuum tape casting machine with a doctor blade which is more suitable for smaller-scale coating operations as shown in Figure 2.2.2.

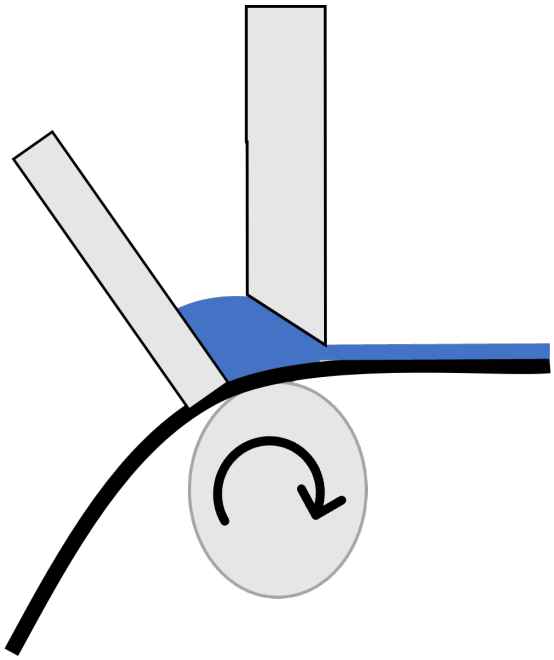

Figure 2.2.2: Simplified illustration of a doctor blade. Figure inspired by [39]
.

Table 2.2.1: Comparison of coating units.

Property	**Comma-bar**	**Slot-die**
Coating speed	Can produce up to 15m of electrode per minute	Can produce up to 80m of electrode per minute
Atmospheric conditions	Exposed to atmosphere	Not exposed to atmosphere
Coating Thickness Control	Limited control	Extensive control

After the coating process, the electrode needs to be dried. The drying process is quite significant for the quality of the finished electrode. Drying too rapidly can cause crack formation and propagation in the electrode, so controlled drying is important. The most common types of industrial dryers are convection dryers, infrared (near infrared) dryers and microwave/laser dryers. The most important parameters for dryers are: (1) temperature profile in dryers, (2) energy required, (3) humidity of incoming air, (4) volume flow rate and (5) routing of air flow. Drying is an energy intensive process so efficiency is important. Some dryers try to recover solvents used to be reused in other electrodes. An example of this is in

a multistage convection drying process [35]. Laboratory drying processes typically involve vacuum drying and vacuum ovens. As mentioned earlier, control of the drying process is important in order to have good quality control of the electrode. Control of the drying process is done by regulating time, temperature and airflow (only with convection drying). The quality measures which indicate how effective the drying was are: (1) coating thickness and weight per area, (2) surface quality and contour, (3) Adhesion strength and (4) residual wetness of the electrode [6].

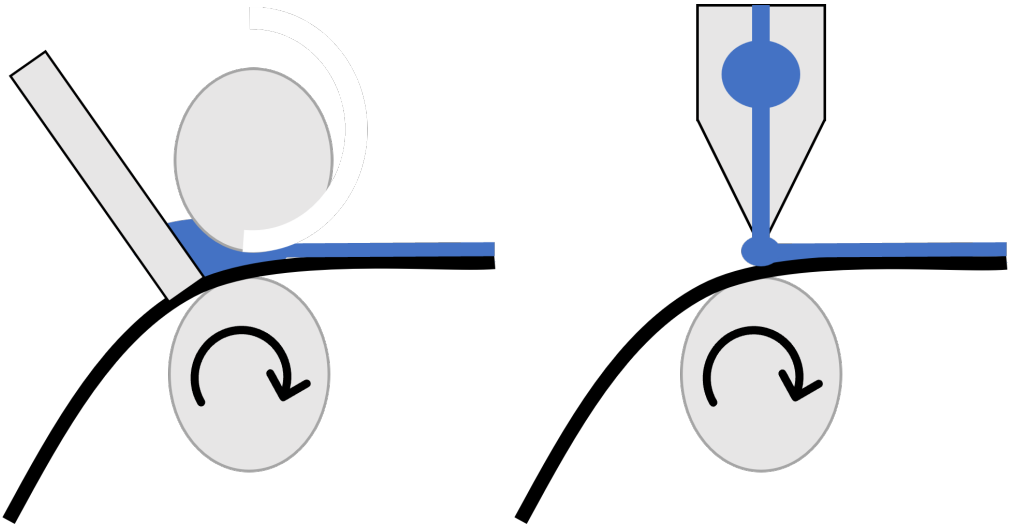

(a) Comma-bar illustration **(b)** Slot-die illustration

Figure 2.2.3: Simplified illustration of coating units. Figure (a) shows an illustration of a comma-bar. Figure (b) shows an illustration of a slot-bar. Figure inspired by [39].

.

Calendaring

Calendaring is the process of compressing the dried electrode material in order to increase material density, increase volumetric energy density and adjust mechanical behaviour [40]. The porous electrodes are driven through two large cylinders and subsequently compressed. This is repeated until the desired thickness and porosity is achieved. The main reasons to calendar electrodes are: (1) thickness control, (2) smoothing the surface and mechanical homogenisation, (3) fixation of pore structure distribution, porosity and tortuosity, (4) fixation of electron transport network and (5) removal of plastic deformation and elastic bonding.

Cutting electrodes

After the electrode sheet has been calendared to the desired thickness, electrodes are cut out into the desired shape. This can be done simply by cutting or punching

out electrodes into desired shape. This is the method often use at laboratory level since it doesn't require complex equipment and can be quite accurate. A different method is using laser cutting which is much more accurate but can cause other issues like a large heat-affected zone or melt formation. Laser cutting is more commonly used on an industrial scale [41].

2.2.2 Cell assembly

The last step in the production process is the cell assembly phase. Cell assembly is a complex process that involves assembling the anode, cathode, separator and electrolyte into a single container. The specific assembly method varies depending on the battery type and performance constraints.There are three main assembly methods which illustrated in Figure 2.2.4.

The first method is called stacking and is the simplest method of assembling a cell. The electrodes and separators are discrete sheets so it is possible to stack layers of flat sheets on top of each other to get alternating cells [5]. This is quite a labour and time intensive process though it does allow for quality control of each layer. A variant of stacking is used when producing coin cells. So components are typically stacked and compressed, with careful consideration given to electrode orientation and electrolyte injection.

Z-folding is similar to stacking in the sense it has discrete electrodes but the separator is continuous. This continuous separator better prevents accidental contact between the electrodes and so lowers the risk of short circuits and possible thermal runaway. The continuous separator makes it less time consuming to produce the cell on an industrial scale. The downside of the continuous separator is the bending stress introduced on the material.The separator needs to be mechanically strong enough to tolerate the bending stress [42]. This method is often used for pouch cells.

Winding is the third method often used on an industrial scale. A winding process is often used for cylindrical and prismatic cells. Winding uses a continuous separator and continuous electrodes. This ensures high output productivity making it a great choice at an industrial scale. Similar to Z-folding, there is the danger of bending stress affecting cell performance. The danger is even higher with winding since bending stress will be even more important in the winding process. In addition to the mechanical challenges, bending stress also correlates to electric resistance between coating and substrate. This is because electron transport depends on the quality of contact between coating and substrate. So due to the electrodes experiencing bending stress, there could be implications for cell performance but this requires further research [42].

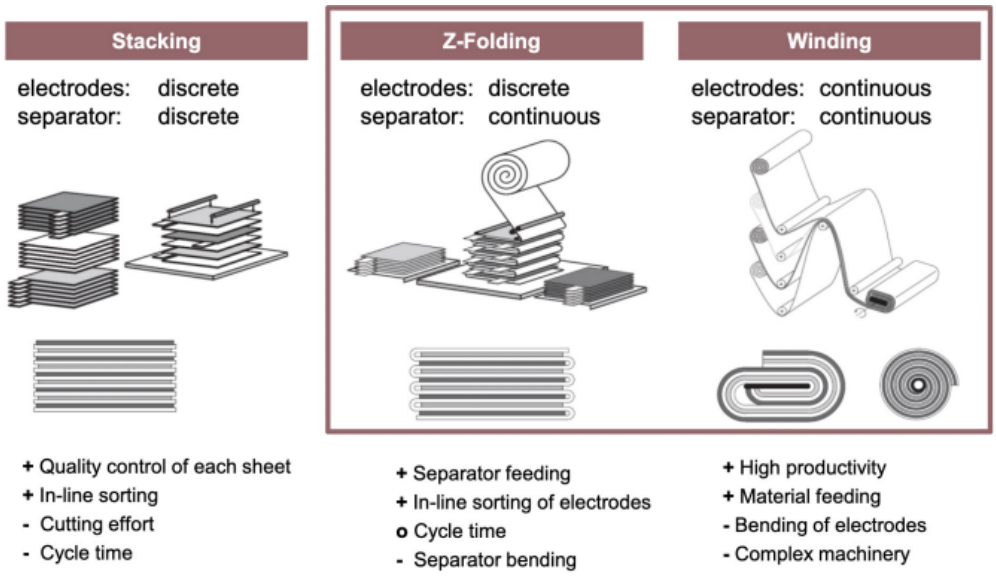

Figure 2.2.4: This is a figure showing the three main assembly methods for LIBs with some advantages and disadvantages. Figure inspired by [42] and [5].

The last step before sealing of the cell is often injection of the electrolyte to maximise electrolyte distribution throughout the cell. Once the electrolyte is injected and the cell assembled, the finished battery is packaged and prepared for formation cycles. Cell formation is the last step before the battery is ready to be delivered to customers. Cell formation refers to the initial charge and discharge of the cell, sometimes also called electrical activation. During formation, the solid electrolyte interface (SEI) is built up [5]. Quality control during cell assembly and formation is crucial to ensuring uniformity and reliability across batches. Factors such as electrode alignment, electrode uniformity, electrolyte amount, and sealing integrity impact the overall performance and safety of the battery [43].

2.3 Electrochemical theory

Electrochemical theory is fundamental to understanding the thermodynamics and kinetics of lithium-ion battery reactions. Standard cell potential and half-cell potential describe the electromotive force generated during electrochemical processes. In lithium-ion batteries, the redox reactions at the anode and cathode contribute to the overall cell potential [5]. Figure 2.3.1 shows an overview of the electrochemical relations essential to understanding how a battery works.

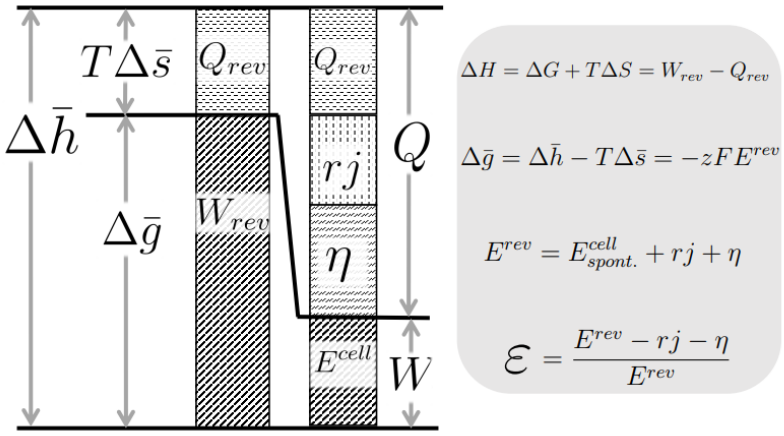

Figure 2.3.1: Figure illustrating key electrochemical relations for an electrochemical device. $\Delta\bar{h}$ represents the reaction energy, also known as enthalpy change. $T\Delta\bar{s}$ is the product of temperature and entropy change. Q_{rev}, W_{rev}, E_{cell}, and η denote reversible heat, reversible work, cell potential, and overpotential, respectively. Figure from Burheim [5].

2.3.1 Standard cell potential and half cell potential

The standard cell potential is a useful indicator of the cell's overall tendency to undergo a redox reaction, with a higher value indicating a more spontaneous reaction. The standard cell potential is the potential difference between positive and negative electrode in an electrochemical device [44] [5].

The standard cell potential (E_{cell}) can be calculated using the Nernst equation under standard conditions as shown in Equation 2.3.

$$E_{\text{cell}} = E_{\text{cathode}} - E_{\text{anode}} \tag{2.3}$$

where E_{cathode} and E_{anode} are the standard reduction potentials for the cathode and anode reactions, respectively. [5]

2.3.2 Half-Cell Potential

Electrochemical reactions can be divided into two halves, each associated with one of the half-reactions occurring at an electrode, known as half-cell reactions. Half-cell potentials are measured against a standard reference electrode, usually the standard hydrogen electrode (SHE). The half-cell potential provides insight into the tendency of a specific redox reaction at an electrode to either gain or lose electrons. The standard cell potential is calculated by taking the difference

between the half-cell potentials of the cathode and anode.The half-cell potential ($E_{\text{half-cell}}$) for a specific half-reaction can be determined using the Nernst equation as shown in Equation 2.4 [5].

$$E_{\text{half-cell}} = E_{\text{standard}} - \frac{RT}{nF} \ln\left(\frac{[\text{Reductant}]}{[\text{Oxidant}]}\right) \tag{2.4}$$

where E_{standard} is the standard electrode potential, R is the gas constant, T is the temperature in Kelvin, n is the number of moles of electrons transferred, F is the Faraday constant, and [Reductant] and [Oxidant] are the concentrations of the reductant and oxidant species.

2.3.3 Overpotentials

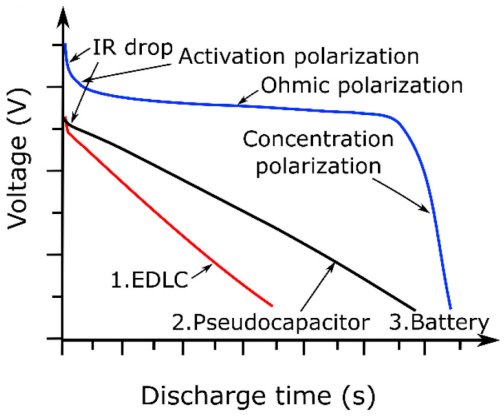

Figure 2.3.2: Figure showing different overpotentials for a battery. Figure taken from Xie et al. [45]

Over-potentials, irreversible losses of potential, are split into three main categories, activation overpotential, concentration overpotential, and resistance overpotential. The activation overpotential is often referred to as the reaction overpotential. Identifying and minimising overpotentials is important for understanding and improving the key factors affecting the performance of lithium-ion batteries. Figure 2.3.2 shows the overpotentials for a battery. Tafel and Butler-Volmer overpotentials are commonly used to graphically represent the reaction overpotential [5].

Another way of displaying the available cell potential of a battery is using the reversible potential. The reversible potential of a lithium-ion battery, E^{rev}, will change with the state of charge (SOC) during cycling. This is due to the concentrations of the reactants and products changing. The remaining cell potential, E^{cell}, at a certain SoC can be defined using Equation 2.5 and Equation 2.6 for discharging and charging respectively.

$$E^{cell} = E^{rev} - rj - \eta_{c.t.} - \eta_{conc.} \tag{2.5}$$

$$E^{cell} = E^{rev} + rj + \eta_{c.t.} + \eta_{conc.} \tag{2.6}$$

where r is the specific resistance, j is the current density, $\eta_{c.t.}$ is the reaction overpotential, and $\eta_{conc.}$ is the concentration overpotential.

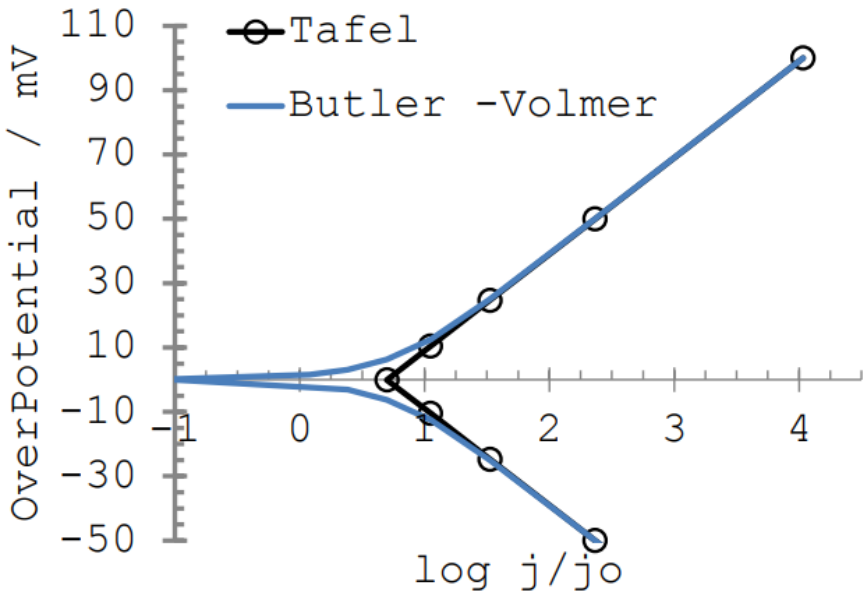

Figure 2.3.3: Figure illustrating Tafel- and Butler-Volmer overpotentials as functions of the logarithm of the ratio between the current density and the exchange current density. Figure from [5].

Activation Overpotential

Activation overpotential, also known as the reaction overpotential or charge transfer overpotential, is the potential difference above the equilibrium potential required to overcome an energy threshold, or activation energy, needed for charge transfer [46]. This activation overpotential directly influences the reaction rates and the efficiency of charge transfer. Charge transfer overpotential relies on the current and is non-linear. Activation overpotential ($\eta_{\text{activation}}$) is related to the exchange current density (i_0) and the actual current density (i):

$$\eta_{\text{activation}} = \frac{RT}{nF} \ln\left(\frac{i}{i_0}\right) \tag{2.7}$$

To fully understand the reaction overpotential, the charge transfer in lithium

ion batteries has to be understood. Charge transfer overpotential is generally described using the Butler-Volmer equation as shown below in Equation 2.8 [47].

$$j = j_0 \left(\exp\left[\frac{\alpha z F}{RT} \eta_{B.V.} \right] - \exp\left[-\frac{(1-\alpha) z F}{RT} \eta_{B.V.} \right] \right) \tag{2.8}$$

where R is the ideal gas constant, T is absolute temperature, F is the Faraday constant, z is the number of electrons per reactant, and α is the symmetry coefficient, where $\alpha = 0.5$.

Concentration Overpotential

Concentration overpotential, stems from the concentration gradient of the reactants or the products in the electrolyte and on the electrode surface. This overpotential becomes significant when the cell reaction is fast enough and when mass transport is restricted [46]. Concentration overpotential ($\eta_{\text{concentration}}$) is related to the concentration of reactants and products as shown in Equation 2.9.

$$\eta_{\text{concentration}} = \frac{RT}{nF} \ln \left(\frac{[\text{Oxidant}]}{[\text{Reductant}]} \right) \tag{2.9}$$

Another way of describing concentration overpotential in terms of concentration gradient is by the reversible potential change at the surface, and the subsequent change in surface concentration, c_s, relative to the concentration in the bulk of the electrolyte, c_b. This is described in Equation 2.10.

$$\eta_{conc.} = -\frac{RT}{zF} \ln \left[\frac{c_s}{c_b} \right] \tag{2.10}$$

Resistance Overpotential

At higher current densities, activation overpotential is no longer limiting. So, resistance overpotential results from the ohmic losses encountered by the flow of current within the various components of an electrochemical cell, including electrodes and the electrolyte. This overpotential is influenced by the electrical resistance of the materials within the cell [48]. Resistance overpotential ($\eta_{\text{resistance}}$) is related to Ohm's law:

$$\eta_{\text{resistance}} = iR_{\text{total}}$$

where R_{total} is the total resistance in the circuit.

2.3.4 Effective mass transfer coefficient

The effective mass transfer coefficient is crucial to understanding the rate of lithium-ion transport within the battery. It describes the ease with which lithium ions move through the electrolyte and electrode materials. Before the effective mass transfer coefficient can be calculated, charge transfer and concentration overpotentials need to be looked at more in-depth. Another way of describing the reaction overpotential and concentration overpotential is using Equation 2.11. Together, they are the difference between the measured cell voltage, ohmic voltage and reversible voltage.

$$\eta_{c.t.} + \eta_{conc.} = E^{rev} - E^{cell} - rj \tag{2.11}$$

The Butler-Volmer equation, Equation 2.8, can be simplified when the overpotentials become quite large,so that the right exponential term of Equation 2.8 becomes negligible. This expression then ends up as shown in Equation 2.12 and is known as the Tafel equation. A graphical representation of the Tafel and Butler-Volmer overpotentials is shown in Figure 2.3.3 [5].

$$\eta_{Tafel} = a + b \log [j] \tag{2.12}$$

Extracting the necessary coefficients, Tafel slope and constant in a log j diagram allows for these to be reintroduced into a simplified Butler-Volmer Equation as shown below in Equation 2.13.

$$j = j_0 \left(10^{\left[\frac{\eta_{c.t.}}{b}\right]} - 10^{\left[-\frac{\eta_{c.t.}}{b}\right]} \right) \tag{2.13}$$

From this it is possible to see whether the measured overpotential can be attributed to charge transfer or not. If the coefficients obtained from the Tafel equation,Equation 2.12 and the corresponding simplified Butler-Volmer equation, Equation 2.13 don't overlap the measured overpotential, then the overpotentials can not be attributed to charge transfer. The presence, or lack, of charge transfer overotential does not exclude the possibility of there being concetration overpotential. The next step towards obtaining the effective mass transfer coefficient is extracting the concentration overpotential as the remaining overpotential using a combination of Fick's law and Coulomb's law [5].

The effective mass transfer coefficient (D_{eff}) can be related to ion diffusion in the electrolyte using Fick's first law:

$$i = -nFAD_{\text{eff}} \frac{dc}{dx} \tag{2.14}$$

where i is the current, n is the number of moles of electrons transferred, F is the Faraday constant, A is the electrode area, D_{eff} is the effective mass transfer coefficient, c is the concentration of ions, and x is the distance.

Combining Coulomb's law with Fick's law expressed in Equation 2.14, Equation 2.15 can be obtained once the concentration overpotential is found.

$$j = -zFJ_{Li} = zFD_{Li}\frac{dc_{Li}}{dx} = zFh_{eff.}c_b\left(1 - \frac{c_s}{c_b}\right) \tag{2.15}$$

where J_{Li} is the molar flux of lithium, D_{Li} is the diffusion coefficient of the Lithium, and dc_{Li}/dx is the concentration gradient.

Finally, combining Equation 2.15 with Equation 2.10, an expression for an effective mass transfer coefficient, h_m can be obtained as shown below in Equation 2.16:

$$h_m = \frac{j}{zFc_b\left(1 - \frac{c_s}{c_b}\right)} = \frac{j}{zFc_b\left(1 - \exp\left[-\frac{zF\eta_{conc.}}{RT}\right]\right)} \tag{2.16}$$

2.3.5 Rate capacity retention

Rate capacity retention is an important phenomena generally defined as a combination of overpotentials and cell cycling. The phenomena refers to the ability of a battery to retain capacity after a certain amount of cycles when compared to the initial maximum capacity of the battery [49]. Finding the initial maximum capacity is done by cycling a battery from a fully charged state to a certain voltage and observing the capacity at incredibly low currents. As shown in Equation 2.5 the cell potential of a battery is lower than the reversible potential when a current is applied. Therefore, the discharge process stops progressively sooner after each cycle, and rate capacity retention can be observed. Rate capacity retention is more noticeable for thicker electrodes and at high C-rates. Rate capacity retention analysis is important because the increase in rate capacity retention is generally attributed to non-ohmic overpotentials. Separating what can be attributed to charge transfer overpotential or concentration overpotential provides an insight into the battery performance.

2.4 Characterisation Techniques

Characterisation techniques are needed to evaluate the performance, state of health, and structural changes of lithium-ion batteries. Researchers employ a variety of methods to assess parameters such as state of charge, state of health, and structural integrity. There are many different types of characterisation techniques. The most common techniques for evaluation of battery cycling are cyclic voltammetry (CV), galvanostatic charge and discharge (GCD), constant current -constant voltage (CCCV) and electrochemical Impedance spectroscopy (EIS).

2.4.1 Battery nomenclature

State of Health

As a battery ages, capacity decreases due to degradation mechanisms. Degradation mechanisms describe irreversible chemical and physical changes happening within the battery [50]. Some examples of these mechanisms are electrolyte decomposition, loss of active material and compromised inter-particle contact at the cathode. SoH is difficult to measure directly since it would require opening a battery in operation which isn't feasible with most battery packs. SoH is generally measured indirectly by comparing currently available battery capacity, $C_{current}$, against rated battery capacity, C_{rated}, i.e. the given battery capacity when it was brand new. This is shown below in Equation 2.17.

$$SoH = \frac{C_{current}}{C_{rated}} \times 100 \tag{2.17}$$

State of Charge

State of charge, SoC, is a common definition for measuring the remaining capacity in the battery [51]. The State of charge is defined as the residual energy capacity, C_r, over the maximum energy capacity of the battery,C_{max} as seen in Equation 2.18. In reality, the remaining energy left in a battery is defined as the current concentration of lithium-ions in the cathode over the maximum possible concentration. For simplicity, it is generally defined as remaining capacity instead of the remaining concentration of lithium-ions. The depth of discharge, or DoD, is usually defined as the percentage of the battery that has been discharged relative to its fully charged state.

$$SoC = \frac{C_r}{C_{max}} \tag{2.18}$$

A more accurate definition of SoC also includes state of health since batteries age and as they age their capacity is reduced. Taking this into account,a new definition of SoC can be defined as shown in Equation 2.19

$$SoC = \frac{C_r}{C_{max} \times SoH} \tag{2.19}$$

There are two main methods used to find the SoC. The first is coulomb counting where charging and discharging currents are measured over time to determine the energy charged or discharged. The second is using the open circuit voltage, or OCV. This is done by measuring the electrical potential between two terminals when disconnected from a circuit.

During characterisation it can be easy to mix up nominal capacity (C_{nom}) and dynamic capacity (C_{dyn}). Nominal capacity represents the amount of charge delivered by a fully charged battery under specified load and temperature conditions [52]. On the other hand, dynamic capacity reflects the battery's actual performance during dynamic operating conditions, accounting for factors like varying discharge rates and temperature effects. This gives us Equation 2.20 and Equation 2.21 to describe nominal and dynamic SoC. The issue with dynamic SoC is the difficulty in accurately measuring it during characterisation.

$$SoC_{\text{dynamic}}(t) = \frac{Q(Dis)}{Q_{\text{max}}} \tag{2.20}$$

In Equation (2.20), $SoC_{\text{dynamic}}(t)$ represents the dynamic State of Charge at time t, $Q(Dis)$ is the specific discharge capacity, and Q_{max} is the maximum charge the battery can hold at a given C-rate.

$$SoC_{\text{nominal}} = \frac{Q(Dis)}{Q_{\text{initial}}} \tag{2.21}$$

In Equation (2.21), SoC_{nominal} represents the nominal State of Charge, $Q(Dis)$ is the specific discharge capacity, and Q_{initial} is the initial charge of the battery.

C-rate

Another important measurement when analysing batteries is how fast it discharges or charges and is known as the C-rate. The C-rate is the power delivered to or removed from the battery per hour divided by the capacity of the battery. It is also defined as the change in SoC per hour divided by hundred as seen in Equation 2.22.

$$C - rate = \frac{\Delta SoC/hours}{100} \tag{2.22}$$

2.4.2 Cyclic Voltammetry

Cyclic voltammetry, CV, is an electrochemical technique which measures the current that develops in an electrochemical cell under conditions where voltage is in excess of that predicted by the Nernst equation. CV provides information about processes at the surface of the working electrodes, such as mass-transport and charge transfer processes [53]. CV is performed by cycling the potential of a working electrode, and measuring the subsequent current. Voltage is adjusted in a controlled manner and the the voltage boundaries are defined by the user [45].

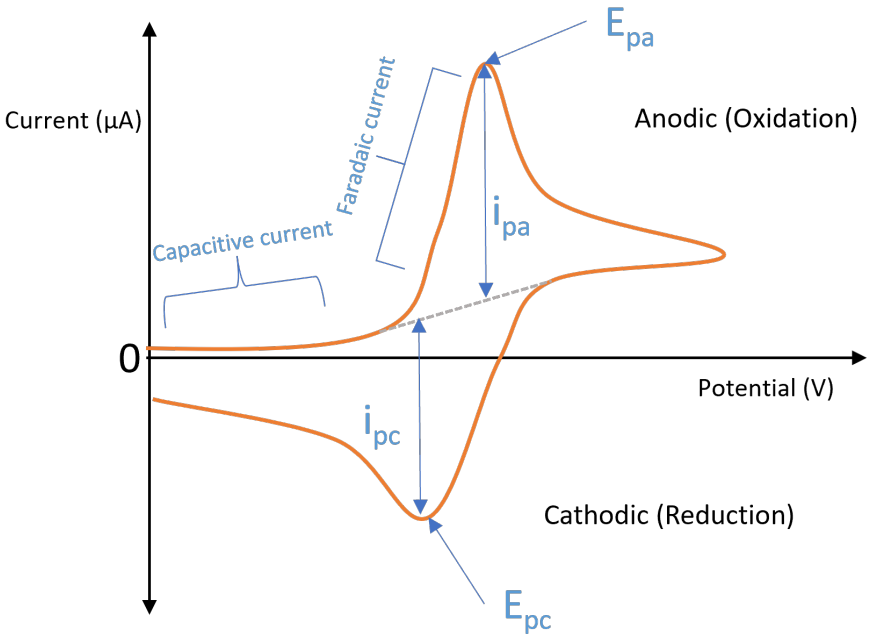

Figure 2.4.1: Figure illustrating cyclic voltammetry of a reversible oxidation process where E_{pa} is peak anodic potential, E_{pc} is peak cathodic potential, i_{pa} is peak anodic current and i_{pa} is peak cathodic current. Figure inspired by [53].

2.4.3 Galvanostatic Charge and Discharge

Galvanostatic charge and discharge, GCD, is an electrochemical characterisation technique where a current is fixed at a constant rate and applied to an energy storage system within a predefined potential limit. This charging and discharging operation is usually performed for multiple cycles [54]. It is useful for comparing voltage against capacity. Voltage is applied and measured in order to maintain current. A GCD plot is typically normalised to the theoretical mass/capacity of the material but doesn't have to be. GCD can be quite informative for capacity and battery behaviors during charging and discharging. Additionally, GCD plots can be used to assess the quality of the capacitive response. GCD is a widely employed method for reliably assessing the rate capability and other performance metrics of batteries [45]. Figure 2.4.2 shows an example of GCD characterisation plots.

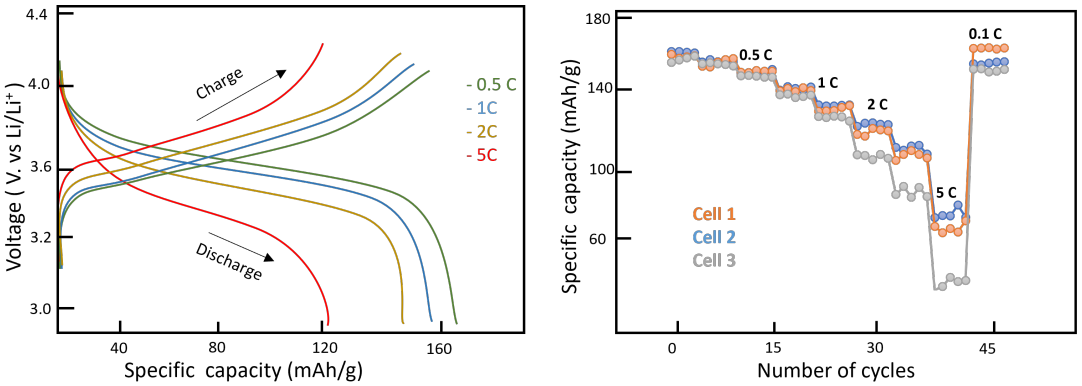

(a) Voltage vs specific capacity **(b)** Specific capacity vs No. of cycles

Figure 2.4.2: Figure illustrating an example of using galvanostatic discharge and charge characterisation to evaluate the performance of batteries at different C-rates. Figure (a) shows a typical result of discharge and charging curves at different C-rates. Figure (b) shows a typical result for comparing rate capability of three different cells after numerous cycles. Figure inspired by [54].

2.4.4 Constant Current - Constant Voltage

Constant Current - Constant Voltage, or CCCV, is a charging method for batteries which is often used for electric vehicles and other types of LIB applications. CCCV consists of two different phases, constant current charging and constant voltage charging. As seen in Figure 2.4.3, CCCV involves initially charging the battery at a constant current until it reaches a predetermined cut-off voltage, then transitions to a constant voltage phase until the current reduces to a predetermined cut-off current [55].

CCCV provides good rate capability at high C-rates and improves overall cycling stability. This makes it useful when doing cycling tests with high C-rates. CCCV characterisation is valuable for assessing key factors such as charging efficiency, capacity, and voltage stability for batteries [56].

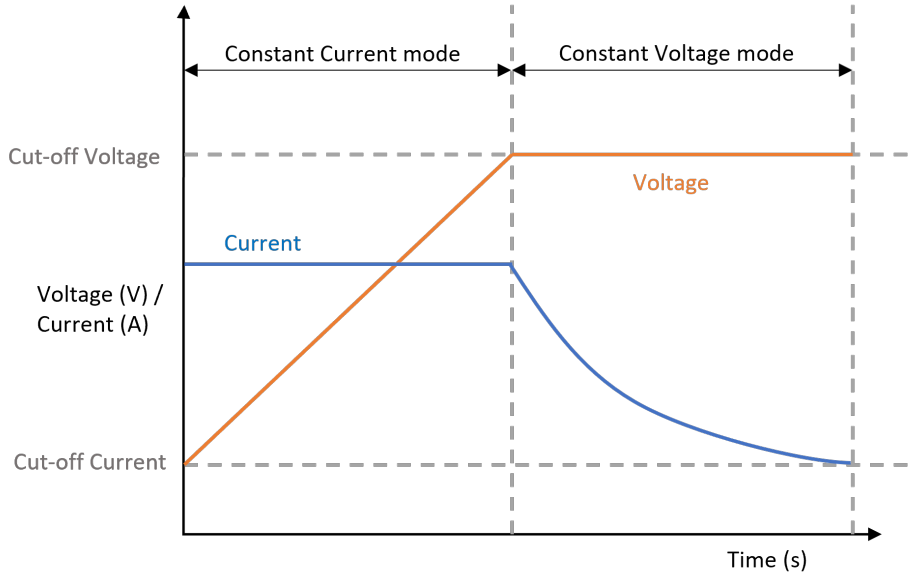

Figure 2.4.3: Figure illustrating a typical result for CCCV characterisation where the x-axis is time (in seconds) and the y-axis is current (Ampere) and Voltage (Volt). Figure inspired by [57].

2.4.5 Electrochemical impedance spectroscopy

EIS, or Electrochemical Impedance Spectroscopy, is a method used to analyse batteries to obtain frequency dependent impedance [58]. It involves applying a low-amplitude alternating voltage signal (typically 5 mV) at OCV on top of a DC potential. This alternating voltage is applied between the working electrode and the reference electrode. It is also possible to perform EIS by applying a current controlled signal (typically 0.5mA) to acquire impedance results [12].

The resulting impedance data is often represented as a Nyquist plot, which commonly exhibits three main regions: an intercept at the real axis (denoted by RE(Z)), a semicircle in the high-frequency range, and a linear portion at low frequencies. This approach assumes that the electrochemical system can be represented by a simple RC equivalent circuit. EIS tells us about the maximum power density, charge transfer resistance and the differential capacitance of a two electrode cell or a three electrode setup with a reference electrode [45].

EIS can also tell us about the different diffusion processes for estimating diffusion coefficients and can provide valuable insight into corrosive mechanisms and corrosion rate of certain materials [59].

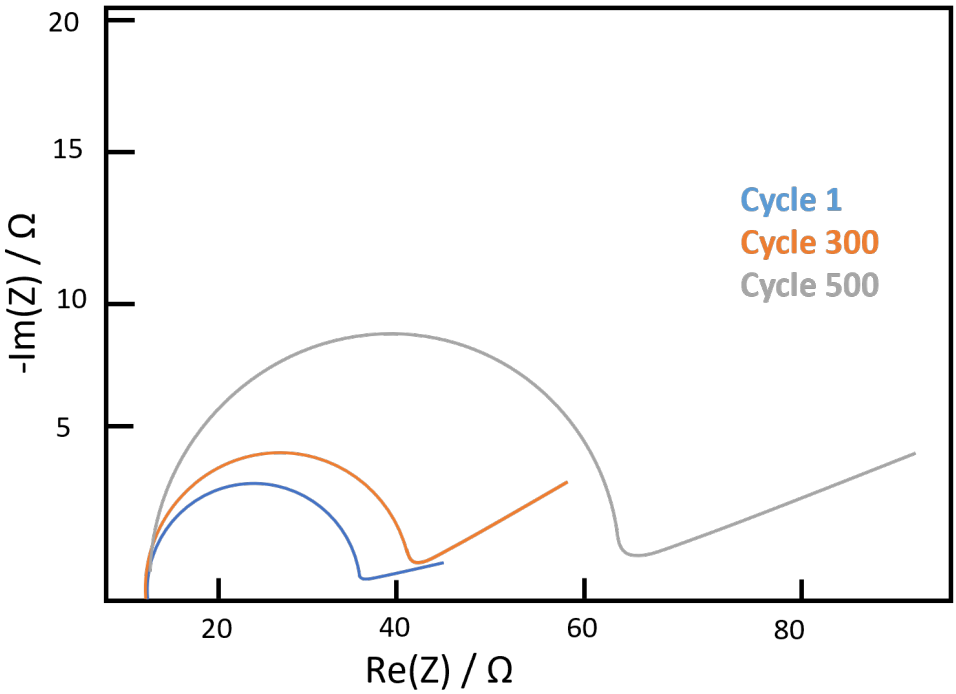

Figure 2.4.4: Nyquist plot illustrating typical result for EIS characterisation. RE(Z) denotes the real axis with resistance (Ohms) and Im(z) denotes the imaginary axis with reactance (Ohms). Figure inspired by [60].

2.4.6 Scanning electron microscopy

Scanning electron microscopy, SEM, is a widely used imaging method to analyse material surfaces at an microscopic level. These microscopes generally have the ability to magnify the material surface up to anywhere from 1 μm to 1 nm. SEM works by firing an electron beam at the material surface and analysing the interaction of these electrons when they hit the material. This interaction causes the electrons to behave in different ways. The two main physical results of this interaction is how the electrons behave. The first one is called back scatter electrons, BSE. BSE are generally high energy electrons that emerge from deeper in the material and often scatter quite vertically. The other main type of electron behaviour is secondary electrons, SE. SE are generally low energy electrons that emerge from closer to the surface than BSE and often scatter at a shallower angle than BSE. These electrons are detected by detectors in the microscopes and are converted to a digital signal that can be shown as an image. For investigating

topographical features, SE usually provide better resolution than BSE but BSE can give elemental contrast since they emerge from deeper in the material. Acceleration voltage and beam current also affect resolution but they can be tweaked to obtain the clearest image while highlighting the topographical features that are of interest [61, 62].

CHAPTER

THREE

METHOD

This section covers methods and materials used during the project and any experimental work performed. First the chemicals and apparatus used during electrode production are presented, followed by a step-by-step process of the battery production process. Next the three electrode setup is presented along with the work done using it. The characterisation of the manufactured cells is described next, including the lithiation of the reference electrode. Finally, the calculation of the effective mass transfer coefficient is described in detail.

3.1 Chemicals and Apparatus

Making the cathode required mixing a slurry of active material, conductive additive, binder and solvent. The active material in the produced cathodes was lithium nickel manganese cobalt oxide (NMC111), where 1:1:1 expresses an equal amount of the three transition metals (Ni, Mn, and Co). The conductive additive used was carbon black. The solvent used was distilled water. The binder used was Lignin, which is non-toxic alternative to PVDF (Polyvinylidene fluoride). Lignin is a polymer which is obtained as a waste derivative of the paper making or pulp industry. The chemicals used are listed below in Table 3.1.1.

Manufacturing of coin cells and the three electrode setups required various tools and apparatus which are listed below in Table 3.1.2.

Table 3.1.1: Chemicals used during cathode production

Chemical	State	function	Supplier	density
NMC111	Powder	Active material	Targray	2.3
Carbon black	Powder	conductive additive	Imerys	1.9
Lignin	Powder	Binder	Sigma Aldrich	1.3
Water	Liquid	Solvent	-	-
Ligning + water	mixture	-	-	-

Table 3.1.2: Table of apparatus used including the model and their function

Apparatus	model	Function
Weight scale	Mettler AE 260 DeltaRange	Weighing chemicals
Mixer	THINKY ARE-250	Mixing the slurry
Heating Type Cast Coater with vacuum	MMSK-AFA-HC100	coating the slurry and calendaring
Electronic Micrometer	IRONSIDE	measuring electrode thickness
Hand-held disk cutter with 15mm circumference	MSK-T-12	Cutting the electrodes
Magnetic stirrer	IKA RCT Classic Magnetic Hot Stirrer	Dissolving binder in solvent
Vacuum Glovebox	Mbraun Labmaster Pro SP	Assembling of cells
Vacuum Oven	Heraeus VT 5042 EK Vacuum Oven	Drying of electrodes

3.2 Battery production

The battery production procedure is listed chronologically in the subsequent sections. The procedure is split into discrete sections to comprehensively describe each step of the process to ensure reproducibility of the experimental work. This process is shown in Figure 3.2.2. Battery production can be split into two main parts, electrode manufacturing and cell assembly. First, the battery production section covers the cathode manufacturing process for the coin cells and three elec-

trode setups produced. The subsequent part of this section, cell assembly, covers the components and steps needed to assemble the manufactured electrodes into the finished products, coin cells and three electrode setups.

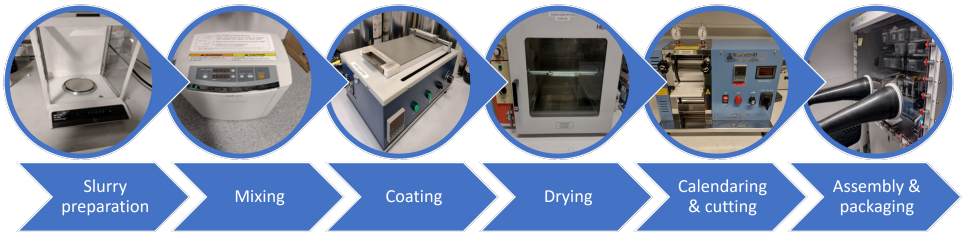

Figure 3.2.1: This is a figure showing the production process for a Lithium-ion battery in a lab.

3.2.1 Cathode manufacturing

The production process for manufacturing the electrodes was fairly consistent for both unstructured and structured electrodes, whether used in coin cells or three-electrode setups. Although there were minor variations at certain stages, which are detailed in the relevant subsections below, these differences were not significant enough to consider the overall production processes as different.

Slurry preparation

The production process for a cathode starts by preparing the slurry that will be mixed together to form the base for the electrode. The slurry preparation consisted of gathering the necessary components, in other words, the binder, conductive additives, solvent and active material to make the slurry. The binder was lignin, which needed to be mixed with a solvent into a liquid solution. The solution consisted of lignin and distilled water with a ratio of 1:10 wt% respectively. This solution was prepared by mixing the lignin and distilled water for a minimum of 12 hours using a magnetic stirrer. The active material chosen for this work was NMC111 in powder form. The conductive additive used was carbon black in powder form. The solvent used was distilled water. The theoretical composition of the cathode was designed to be 90:5:5 wt%, consisting of 90% NMC111, 5% lignin/water solution, and 5% carbon black by weight.

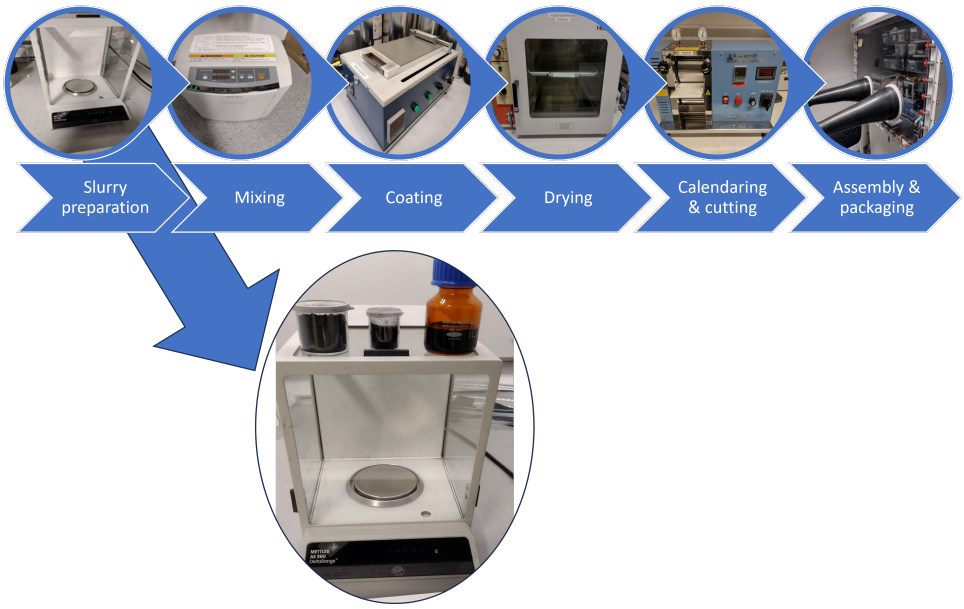

Figure 3.2.2: This is a figure showing some of the apparatus used in slurry preparation for a Lithium-ion battery in a lab. Located on top of the scale are the main ingredients for a lignin based electrode. From left to right, (a) NMC111, (b) Carbon black and (c) Lignin and water solution.

Mixing and dispersion

The next step was to mix the slurry into one homogeneous paste in a two step process so the slurry could be coated onto a current collector in the coating process. To begin with, a "Thinky" mixing cup was placed onto a Mettler AE 260 DeltaRange weighing scale and zeroed before adding 0.4889 grams of the lignin and water solution. Then 0.0444 grams of carbon black were added to the "Thinky" mixing cup. The mixing cup was then locked into place in the Thinky ARE-250 mixer. The mixing program consisted of three cycles of 10 minutes, for a total of 30 minutes, at different mixing speeds. Once a cycle finished, the next cycle would start immediately until all the cycles had been run. The first cycle was set to run for 10 minutes at 1000 revolutions per minute (rpm). The second cycle was set to run for 10 minutes at 2000 rpm. The last cycle was set to run for 10 minutes at 1000 rpm.

Figure 3.2.3: This is a figure showing the mixing equipment for a Lithium-ion battery in a lab. The slurry is placed inside the "cupholder" which is then secured in the larger "cubby".

Once the mixing program was finished, the mixing cup was removed from the mixer and 0.800 grams of NMC111 was measured out and added to the mixing cup. Lastly, 0.4444 grams of distilled water was added to the mixing cup to achieve a powder to liquid ratio of 1:1. After the last ingredients had been added, the mixing cup was placed into the mixer and the same mixing program as described above was run for 30 minutes.

Table 3.2.1: Table of chemical makeup of active material

Chemical	**mass(g)**	**mass ratio**
NMC111	0.8	90
Carbon black	0.0444	5
Lignin	0.0444	5
Lignin:water (1:10 5wt lignin)	0.4889	-
Extra water	0.4444	-

Coating and structuring

After the slurry had been mixed, it was ready for the coating process. The coating process was done on a type cast coater with heating and vacuum control. The first step was placing the current collector sheet on the tape caster. The current collector was a sheet of aluminium foil with a layer of carbon black on top of it for added adhesive strength. After the current collector had been placed on the tape caster, the heating and vacuum were turned on. The vacuum allowed the current collector sheet to lay flush and completely flat on top of the tape caster without being able to move. The slurry was then coated onto the current collector with the desired thickness using the tape caster and a doctor blade with an adjustable gap to select the desired thickness.

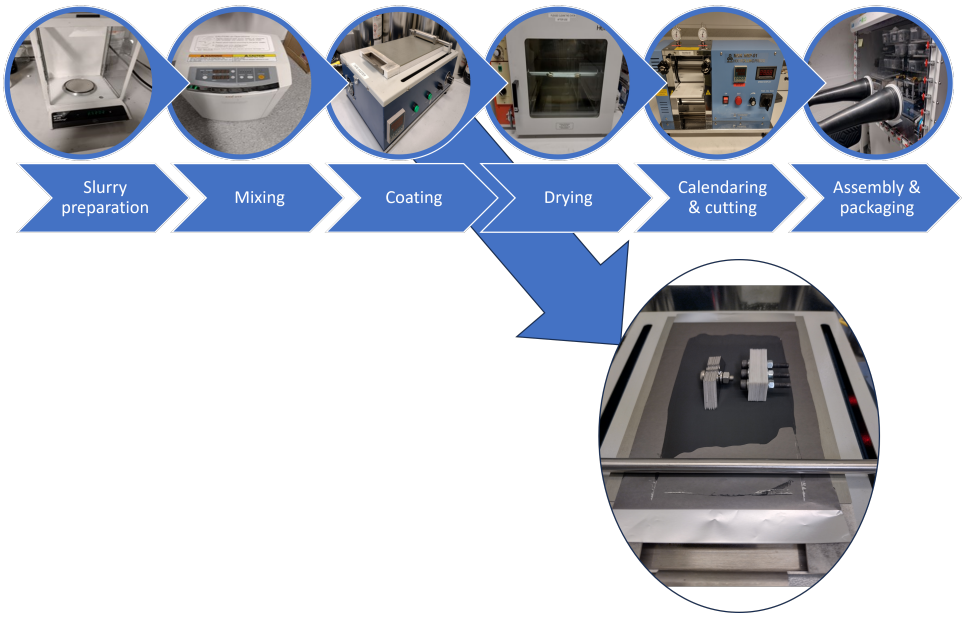

Figure 3.2.4: This is a figure showing an electrode directly after coating and once the structuring process was underway. Once the coating process is complete, after a predetermined time the structuring equipment is placed on the electrode. The picture shows (a) metal structuring blades on the left and (b) ceramic structuring blades on the right.

The structuring process took a lot of trial and error to learn the optimal timing for creating corrugations. If the structuring tools were placed on the slurry too quickly, then too much active material was often removed. If the structuring tools were placed too slowly, then the slurry had dried enough that the structuring tools were not able to create corrugations. An added layer of difficulty is that some of the structuring tools needed to be placed earlier/later than others. For the metal and ceramic blade structuring tools pictured in Figure 3.2.4, the optimal standard operating procedure (SOP) was found after numerous attempts. The optimal SOP

was found to be placing the structuring tools 3 seconds after the coating process had finished and then leaving it undisturbed for 10 minutes to allow it time to set.

Another structuring tool used was a circular sheet which created circular perforations on the electrode surface, however it did not end up being used for perforations due to the difficulty in finding a good SOP. Figure 3.2.5 shows an example of the different results due to a few seconds of difference when placing the structuring tool.

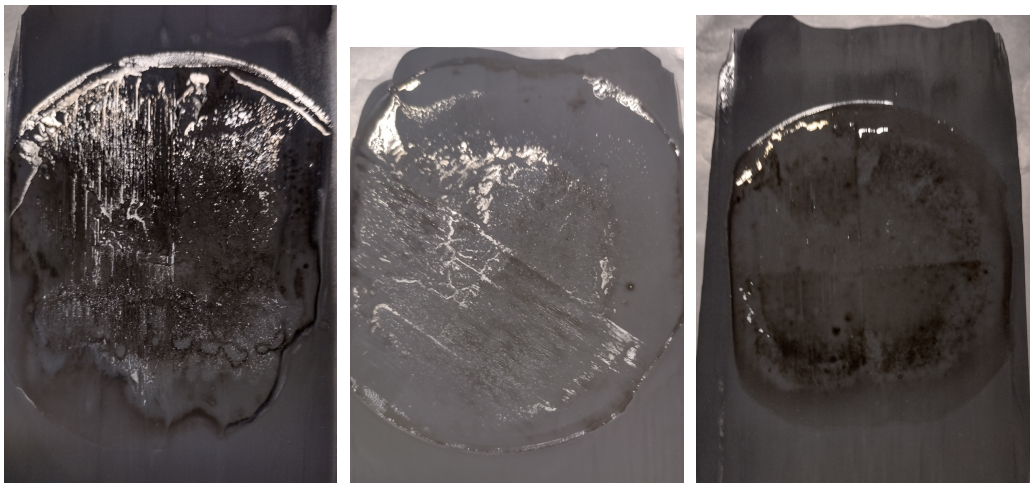

(a) **(b)** **(c)**

Figure 3.2.5: Image (a) shows the electrode surface after a structuring tool was placed on it too quickly resulting in large loss of active material. Image (b) shows the electrode surface after a structuring tool was placed on it slower than (a) but still relatively quickly resulting in mediocre loss of active material.Image (c) shows the electrode surface after a structuring tool was placed on it a few seconds later than (b) resulting in small loss of active material.

Drying

The drying process involved placing the electrode in a vacuum oven to remove any excess water on the surface of the electrode. The electrode was then dried at 50 °C for a minimum of 12 hours in vacuum. Figure 3.2.6 shows an image of the oven vacuum oven used.

Figure 3.2.6: This is a figure showing the vacuum oven used for drying of the electrodes after coating.

Calendaring and cutting of electrodes

Before calendaring, the thickness of the electrode film was measured at several points using a micrometer to ensure homogeneity. Calendaring was then performed until the film reached the desired thickness, based on an ideal porosity of around 30%. The apparatus used for calendaring is shown in Figure 3.2.7. Once the desired porosity was achieved, the electrodes were cut out using a hand-held disk cutter with a circumference of 15mm. The thickness of the cut electrodes was measured again, and then they were weighed to determine the mass of each electrode. These measurements were used to calculate the porosity and specific capacity. After all electrodes were cut and measured, they were ready to be assembled into a coin cell in the glove box.

3.2.2 Cell assembly

Cell assembly took place in a glovebox specifically designed for cell manufacture. The glovebox was filled with argon gas and had an oxygen- and water-controlled atmosphere, with an ideal oxygen content of less than 0.1 ppm and an ideal water content of less than 0.1 ppm. The glovebox is pictured below in Figure 3.2.8.

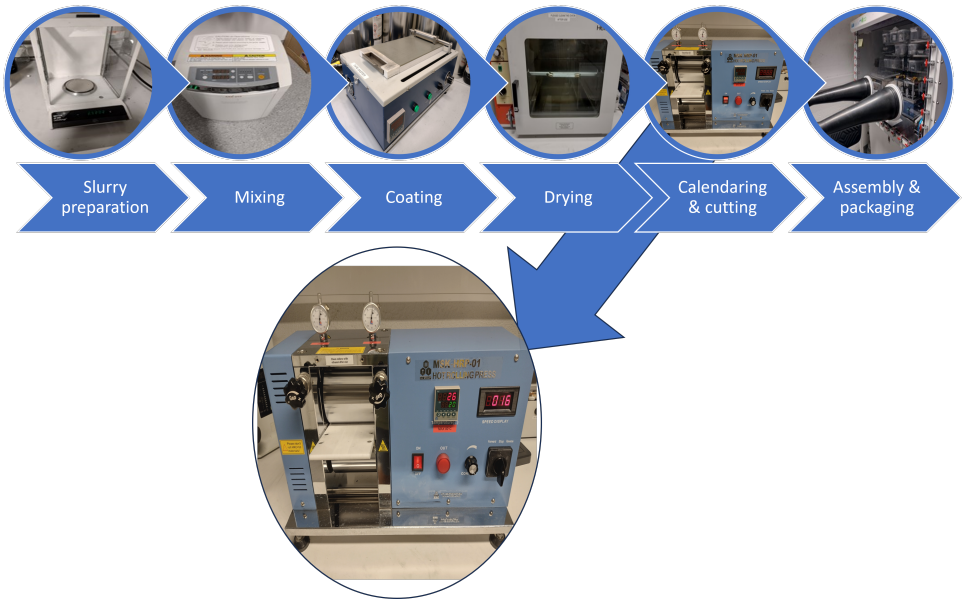

Figure 3.2.7: This is a figure showing the Calendaring apparatus used in the lab.

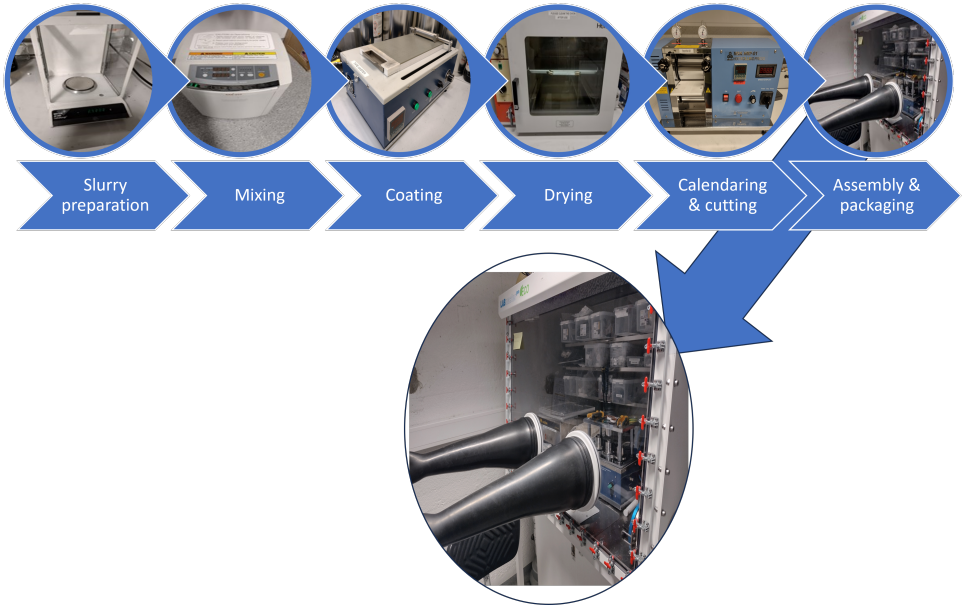

Figure 3.2.8: This is a figure showing where the assembly of cell occurred, in the glovebox.

Coin cell

The assembly of the coin cell consisted of the following equipment: Cathode, spacer, O-rings, anode (lithium metal), separator, electrolyte and containing caps. O-rings and spacers were used to ensure a tight fit. The electrolyte used was a 1:1:1 EC:DMC:DEC mixture with 1M LiPF6 and 40μL of this electrolyte was used during assembly. The electrolyte was added in two stages to maximise wetting throughout the cell. The separator was made of polypropylene and polyethylene. The steps to assemble a single coin cell went as follows:

Step 1. First the stainless steel containing cap for the anode was placed on a clean surface inside the glovebox.
Step 2. A stainless steel O-ring spacer was placed inside the cap.
Step 3. Next the lithium metal anode was placed on top of the O-ring.
Step 4. Next 20μL of the electrolyte was introduced.
Step 5. The separator was added on top of the anode.
Step 6. Once the separator was in place, 20μL more of the electrolyte was added.
Step 7. Next the cathode was placed on top of the separator.
Step 8. Once the cathode was in place, a stainless steel spacer was fitted on top.
Step 9. The last item to be added into the cell was the second O-ring on top of the spacer.
Step 10. The top containing cover was then placed on the cell.
Step 11. Lastly the finished cell was crimped at 861 kPa.

Three electrode setup

The three electrode setup consisted of a reference electrode, a gold wire, a plastic support structure that encases the three electrode setup and is made of Teflon (Polytetrafluoroethylene), a lithium metal anode and a NMC cathode. The reference electrode was a gold wire with the following dimensions: 0.5mm diameter and 4cm in length. The anode was lithium metal. The cathode was an electrode made up of NMC, carbon black, lignin and water with the exact same specifications as the ones made for the coin cells. The only difference in the cathode was the diameter due to size constraints of the TES.

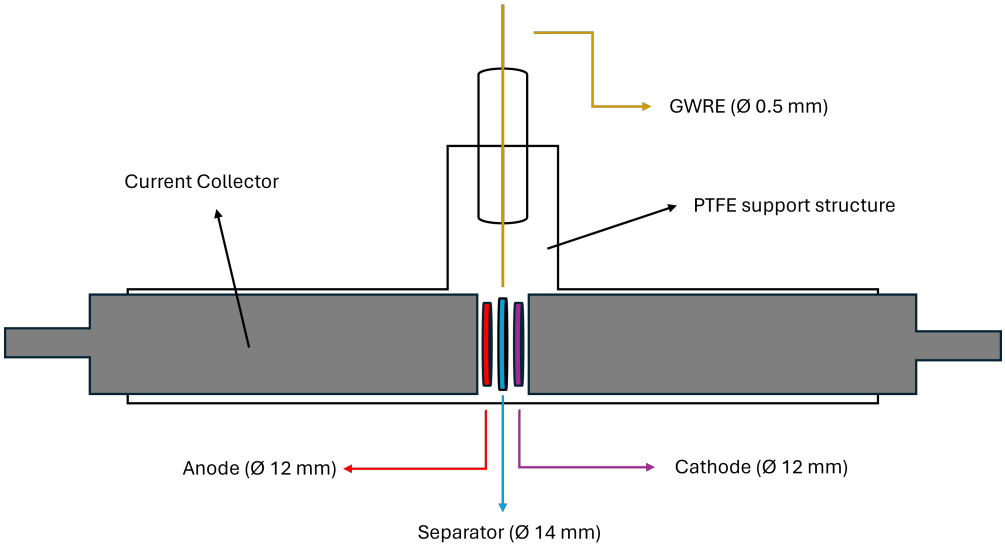

Figure 3.2.9: Illustration of a three electrode setup used containing anode, cathode and reference electrode.

Before assembly of the three electrode setup (TES) could begin, the gold wire had to be fixed to the plastic support structure. This was done by glueing the gold wire at the joint on the top side. The TES was then left overnight to allow the glue enough time to dry and ensure strong adhesion between the gold wire and the plastic support structure. Subsequently the TES was ready for assembly in the glovebox. The TES was assembled in the glovebox just as the coin cells were. The plastic support structure was washed and dried before being brought into the glovebox. One of the current collectors was then removed from the support structure to be able to add electrodes, separator and electrolyte. The removed current collector was then screwed back into the support structure sealing the electrochemically active components inside the support structure.

The separator had a diameter of 14mm and the electrodes had a diameter of 12mm. Before the assembled TES was removed from the glovebox, a multimeter was used to check the open circuit voltage (OCV) to ensure it was ready for lithiation and cycling. When no potential was observed between the gold wire reference electrode and a working electrode, the most common culprit was a lack of electrolyte. Unscrewing the reference electrode then allowed for more electrolyte to be added, which often addressed the issue. Once assembly and testing with the multimeter was complete, the TES could be removed from the glovebox and was then ready for testing operations as shown in Figure 3.2.10.

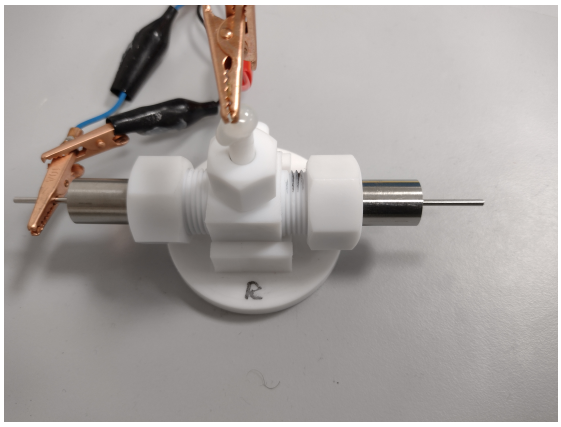

Figure 3.2.10: Image of a three electrode setup undergoing lithiation.

3.3 Characterisation

3.3.1 Scanning Electron Microscopy

Scanning Electron Microscopy, SEM, was used to assess whether the structured electrodes had sufficient corrugations. The SEM characterisation was an important part of the experimental process since it determined if the electrodes could be brought into the glovebox for assembly. The SEM model used was the SEM Apreo from the manufacturer FEI. All samples were subject to an acceleration voltage of 13 kV and the working distances were set between 10 and 20 mm. The surfaces of the electrodes were inspected at various different magnifications to assess the structural integrity of the corrugations. Once the samples had been inspected and approved, they could be assembled into cells.

3.3.2 Cycling

Once the cells were assembled, the cycling process could begin. Wetting time for the cells was generally 7 days to keep it as consistent as possible. In order to analyse the manufactured cells, characterisation methods were applied to the cells. The two main methods of characterisation used during cycling were galvanostatic charge and discharge, or GCD, and constant current-constant voltage, or CCCV. The main purpose of the GCD cycling was to analyse the rate performance of the different cells. The main purpose of the CCCV cycling was to improve cycling stability at high C-rates, since the mass transport cycling schedules used included high C-rates. Figure 3.3.1 shows the equipment used for cycling the coin cells, the LanheCT3002A (Land Battery testing system & data processing software). Cyclic voltammetry and electrochemical impedance spectroscopy were also planned for the three electrode setup but due to time constraints, these methods were not used.

Figure 3.3.1: This is a picture showing the LanheCT3002A - Land Battery testing system & data processing software used for cycling the coin cells

Rate performance schedule

The rate performance schedule shown in Figure 3.3.2 was initially used with purpose of investigating the capacity retention and rate performance of the cells. The coin cells were discharged at different rates during certain parts of the cycle. When the discharging rate was between 1C and 5C, the charging rate was kept at 0.5C. This was done to prevent the battery from being overcharged and potentially damaging it. Charging generally happens faster than discharging so the battery could get charged too quickly if it operated at the same C-rate as the discharging rate. The coin cells were charged to 4.3V and discharged to 3V. CCCV was used between charging and discharging at 4.3V until the current reached the cut-off C-rate at 0.1C.

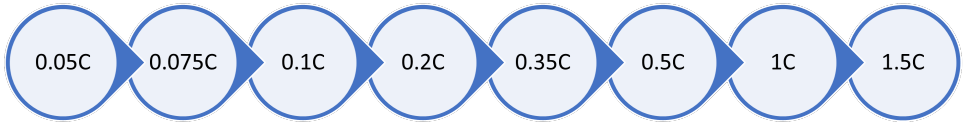

Figure 3.3.2: This is an illustration of the rate performance schedule showing the C-rates for each step in each circle. Each C-rate circle corresponds to 4 cycles for a total of 44 cycles.

Mass transport schedule

The mass transport schedule shown in Figure 3.3.3 was initially used for acquiring results which could be used to determine the effective mass transfer coefficient. Over time it became clear that the mass transport should also be used to investigate rate capacity retention so it could be related to mass transport behaviour at high C-rates. As with the rate performance schedule, the cells were charged to 4.3V and discharged to 3V. CCCV was used between the charging and discharging at 4.3V until the current reached the cut off C-rate at 0.05C. Unlike the rate performance schedule, the discharging and the charging rates did not differ during the cycling.

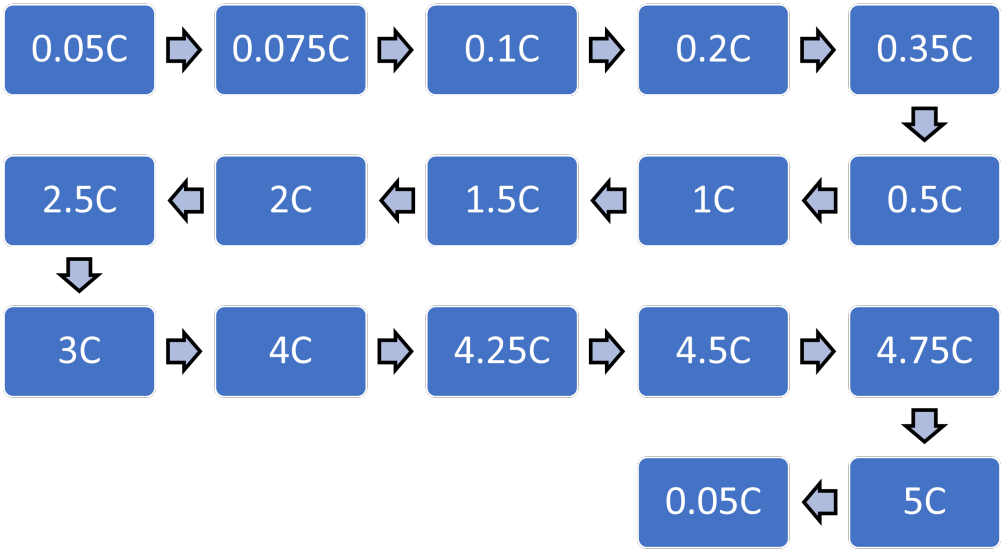

Figure 3.3.3: This is an illustration of the mass transport schedule showing the C-rates for each step in each block. Each C-rate block corresponds to 2 cycles, except for the first C-rate (0.05C) which has 4 cycles, for a total of 38 cycles.

Lithiation of reference electrode

After assembly of the three electrode setup (TES) in the glovebox, the TES was ready for testing. The first step in the testing procedure was lithiation. The GWRE was lithiated over a period of 2 hours by applying a current of 0.005mA between the lithium anode and the GWRE. The lithiation process is the same for the Li/Li^+ and Li/NMC setup. The lithium electrode is the working electrode for both setups. Once the GWRE had been lithiated twice in two different identical TESs using Li/Li^+, the Li/NMC setup was used. Due to the time-consuming nature and difficulty of obtaining results using the TES, the Li/NMC setup was tabled for further work (without obtaining enough reliable results) in order to focus on acquiring enough data to be able to accomplish a thorough mass transport

analysis. The results of this work are shown in the appendix.

3.4 The effective mass transfer coefficient

Obtaining the effective mass transfer coefficient was a complicated process. This section will provide an overview of the steps required using an example data set to showcase the method used during this work. The example data set can be regarded as ideal. In reality the data is distorted due to noise which is especially true at lower C-rates. The first step consists of cycling the cells as described in the previous sections to obtain discharge capacities for a cell discharged using CCCV characterisation methods. Figure 3.4.1a shows an example of what these results could look like. Once the recorded discharge capacities are obtained, the relative discharge capacity can be plotted against cycle number but should also include the C-rates of the different cycles. Figure 3.4.1b illustrates what a relative discharge capacity plot should look like. Relative discharge capacity is defined as the measured capacity at any C-rate divided by the maximum capacity, which is the capacity at infinitely low current. Relative discharge capacity is used to make it easier to compare results of electrodes of different thicknesses and other significant differences which affect their discharge capacities.

In this analysis, the State of Charge, SoC, is often referenced and refers to the nominal SoC as defined in the theory section of this paper. Cell potentials are also extracted at constant nominal SOC, as shown by the greyed-out area in Figure 3.4.1a.

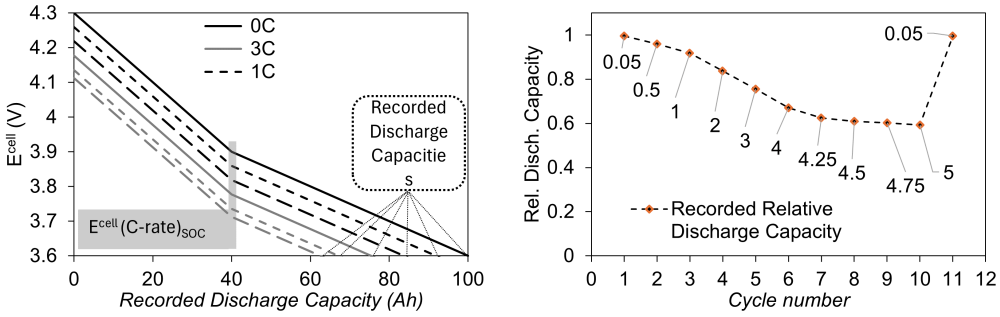

Figure 3.4.1: Figure (a) shows an example plot of measured cell voltage as a function of recorded discharged capacity during discharge. Figure (b) shows an example plot of the relative discharge capacity as a function of cycle number alongside c-rate for each data point.

The next step in the analysis requires calculating the ohmic, (rj), and the charge transfer, $(\eta_{c.t.})$, resistance. When plotting the cell potential as a function of the C-rate as shown in Figure 3.4.2a, the ohmic resistance can be extracted

from within the linear region. Combining the ohmic resistance extracted with Equation 2.11 provides the data needed to plot Figure 3.4.2b. A suggested Tafel fit is obtained by fitting the highest linear non-ohmic overpotential values as shown in Figure 3.4.2b. Using Equation 2.12, the a and b coefficients can be extracted and used in Equation 2.13. This is graphically illustrated in Figure 3.4.2c.

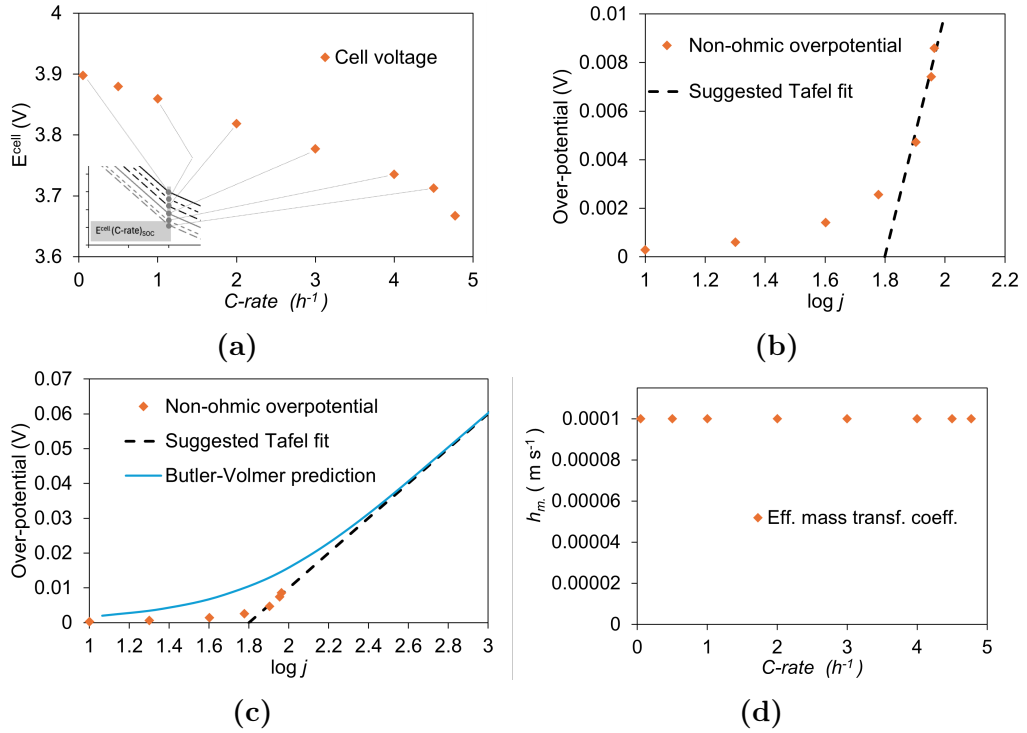

Figure 3.4.2: Figure (a) shows the cell potential as a function of c-rate. Figure (b) shows the measured non-ohmic overpotential as a function of the logarithm of the current density with a Tafel line fit. Figure (c) shows measured non-ohmic overpotential as a function of the logarithm of the current density with a Tafel line fit and a Butler-Volmer prediction. Figure (d) shows the calculated effective mass transfer coefficient as a function of c-rate.

The last step is recognising that the overpotential is not due to charge transfer overpotential since the overpotentials would have to be considerably higher and match the Butler-Volmer prediction as shown in Figure 3.4.2c. Since the non-ohmic overpotential is not charge transfer overpotential, it has to be concentration overpotential. Using Equation 2.16, the effective mass transfer coefficient can be calculated and plotted as shown in Figure 3.4.2d.

CHAPTER

FOUR

RESULTS AND DISCUSSION

This section covers the results of the experimental work performed during this research alongside a comprehensive discussion of these same results. The section is divided into several subsidiary sections. First, scanning electron microscopy images are presented which show the surfaces of the unstructured and structured electrodes. After that, a comparison of rate capacity retention is performed on unstructured and structured electrodes of different thicknesses. The latter half of this section is comprised of a mass transport analysis of unstructured and structured electrodes of various thicknesses, which includes discussion of concentration over-potential and its relation to the effective mass transfer coefficient. Lastly, the results from the three electrode setup are presented and discussed.

4.1 Scanning Electron Microscopy

Structuring electrodes was a cornerstone activity for this research which made the use of Scanning Electron Microscopy (SEM) indispensable. SEM was a necessary tool to ensure thorough and accurate structuring of electrodes during the production process. Figure 4.1.1 shows the surface of an unstructured electrode. From the image it is clear that the surface is quite uniform and there are no structures or other topographical features present on the electrode.

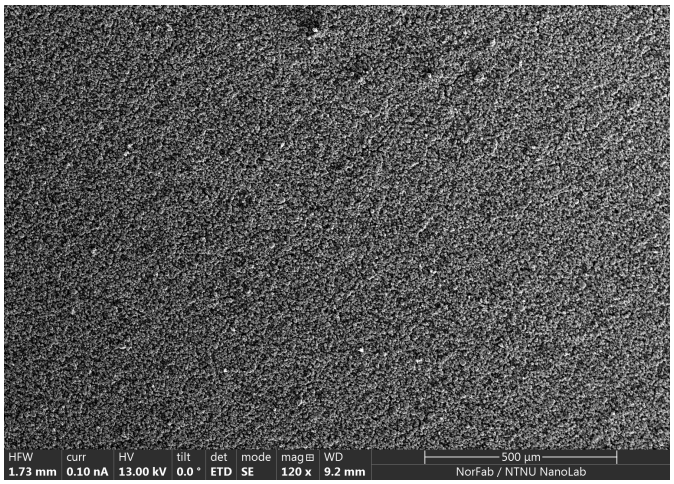

Figure 4.1.1: Figure shows a SEM image taken at 120 times magnification with an acceleration voltage of 13kV.

Figure 4.1.2a shows the surface of a structured electrode. The SEM image clearly shows the indentations made by the structuring tool. Due to the imprecise nature of mechanical structuring, the structures in the material were not completely uniform. The depth of the structures were quite uniform but the width of the indentations ranged from 25 μm to 32 μm. Figure 4.1.2b shows a close-up of one of the structures. As can be seen on the image the structure is not completely uniform throughout. These were only microscopic variations and not enough to cause a marked difference on rate capability or mass transfer results when testing similarly structured cells.

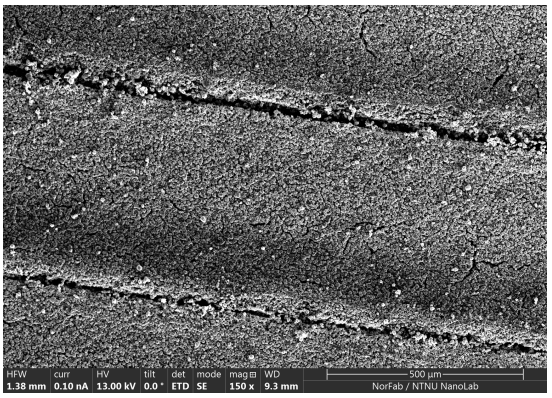

(a) SEM image of structured electrode surface.

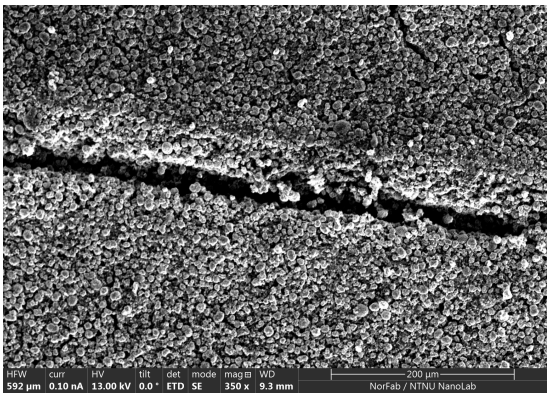

(b) Close-up SEM image of structured electrode surface.

Figure 4.1.2: Figure shows two images of a structured electrode surface. Figure (a) shows SEM image taken at 150 times magnification with an acceleration voltage of 13kV. Figure (b) shows SEM image taken at 350 times magnification with an acceleration voltage of 13kV.

It was necessary to inspect the electrodes and ensure structuring had occurred since it could not be deduced accurately with the naked eye. There were multiple

instances were the electrodes were not structured or only structured partially due to the precise timing required. Additionally, the opposite problem also occurred, were too much active material was removed during the structuring process.

4.2 Rate capacity retention

Rate capacity retention analysis was performed on electrodes of different thicknesses in this thesis. Some of the electrodes were structured, and some were unstructured. This was done to see the effect of structuring on rate capacity retention. The analysis was performed using relative specific discharge capacity when comparing unstructured to structured electrodes of the same thicknesses. This was done to better observe the changes at higher C-rates. The analysis starts with a look at the thinner electrode, 100 μm, and transitions into a look at the thicker electrode, 150 μm. The aim of this analysis is to examine the impact of electrode thickness and structures on the surface of the electrode on capacity retention.

An important note about the electrodes produced is that they weren't completely uniform. The electrodes denoted as 100 μm thick electrodes in this analysis ranged in thickness from 97 μm to 104 μm. For the purpose of this analysis they are all labeled 100 μm thick electrodes. Similarly, The electrodes denoted as 150 μm thick electrodes in this analysis ranged in thickness from 141 μm to 158 μm. For the purpose of this analysis they are all labeled 150 μm thick electrodes. The reason for using multiple types of structuring was to ensure production inaccuracies and discrepancies didn't hinder the analysis of the structured electrodes.

4.2.1 100 μm electrodes

Figure 4.2.1a shows the average rate performance of the thinner tested unstructured electrodes. These electrodes were 100 μm thick and run through 38 cycles at incrementally increasing C-rates. Figure 4.2.1a shows the specific discharge capacity (mAh/g) against the C-rate. Coulombic efficiency is also shown against C-rate. As can be seen in Figure 4.2.1a and Figure 4.2.1b there is a marked reduction in rate performance as C-rate increases. This is especially apparent when transitioning from low C-rates, less than 1C, towards higher C-rates. Figure 4.2.1b is the same data but plotted as relative specific discharge capacity against C-rate. This was done so it would be easier to visualise the differences in capacity retention at various C-rates for different electrodes. Figure 4.2.1b can then be easily compared to the structured electrodes of the same thicknesses and highlight capacity retention differences.

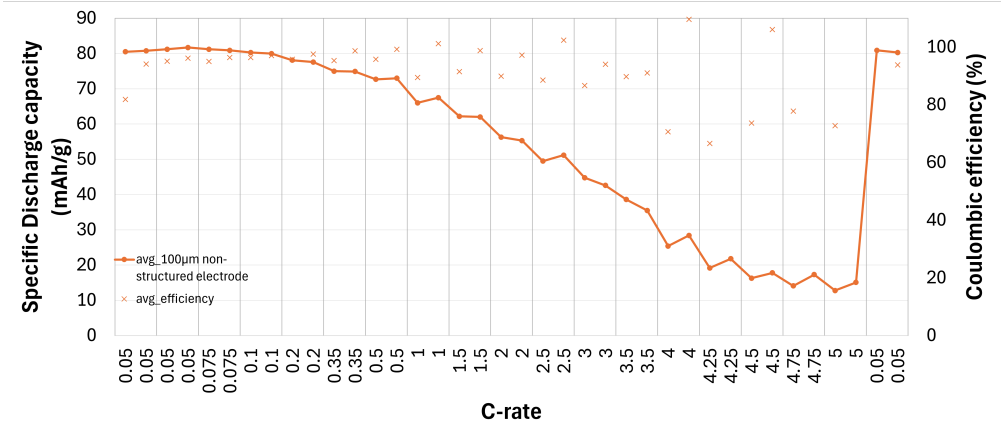

(a) Specific discharge capacity of 100 μm unstructured electrode

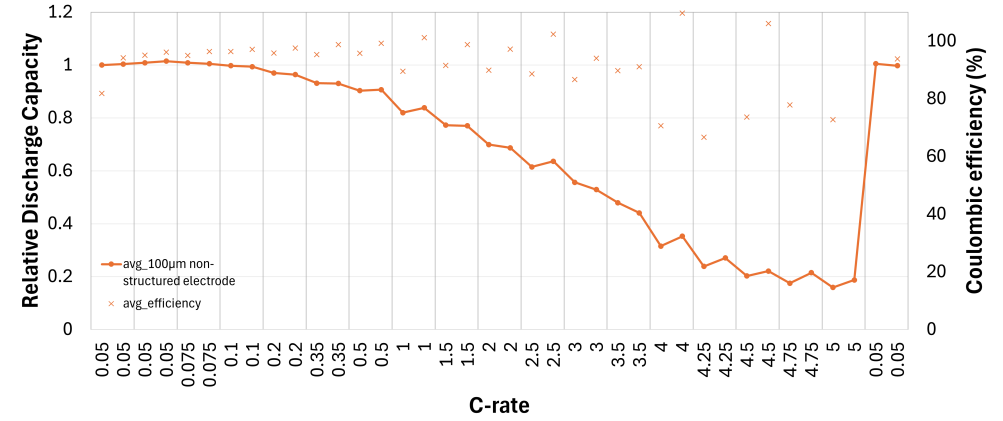

(b) Relative discharge capacity of 100 μm unstructured electrode

Figure 4.2.1: Average rate performance of unstructured 100 μm thick electrodes. Figure (a) shows specific discharge capacity and coulombic efficiency against C-rate. Figure (b) shows relative discharge capacity and coulombic efficiency against C-rate.

Figure 4.2.2a shows the relative specific discharge capacity of a structured electrode using the ceramic blades (CB) used for structuring. The CB structured electrodes show a noticeable difference in capacity retention compared to the unstructured electrode shown in Figure 4.2.1b. At lower C-rates, less than 1C, the rate performance decreases slightly faster than an unstructured electrode does but not considerably. On the other hand, at medium and high C-rates the capacity retention is notably higher. Figure 4.2.2a visibly shows this as the relative specific discharge capacity stays between 60% and 40% at C-rates ranging from 1C to 5C. This is a distinct difference to Figure 4.2.1b where the relative specific discharge capacity drops rapidly from 75% to down to around 20% once the C-rates ramp up past 1 C. This can also be seen in figure Figure 4.2.2b which shows the relative specific discharge capacity of a structured electrode using the metal blades (MB) used for structuring. This data also clearly shows a significant improvement in capacity retention at higher C-rates. The relative specific discharge capacity remains within a range of 62.5% to 40% at higher C-rates ranging from 1C to 5C.

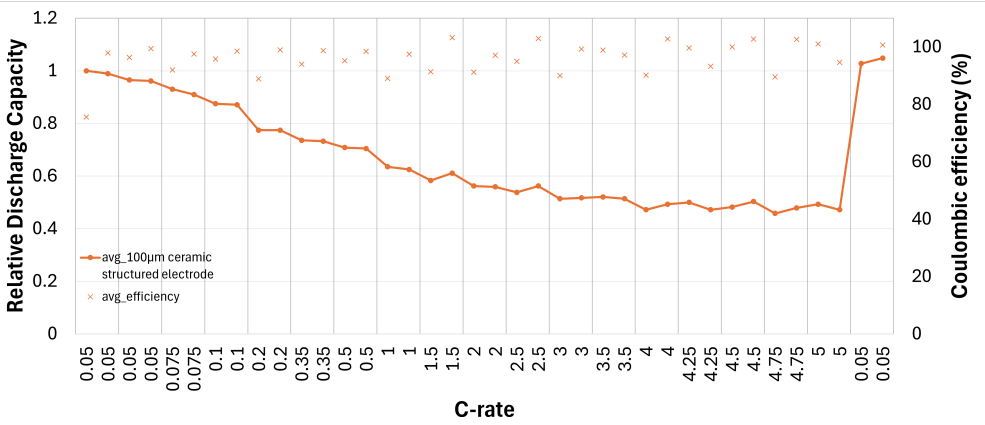

(a) Relative discharge capacity of 100 μm ceramic structured electrode

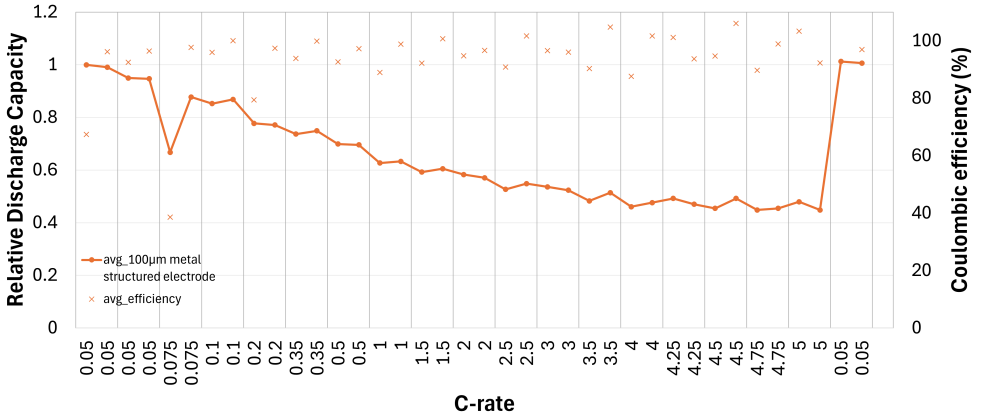

(b) Relative discharge capacity of 100 μm metal structured electrode

Figure 4.2.2: Average rate performance of structured 100 μm thick electrodes. Figure (a) shows relative discharge capacity and coulombic efficiency against C-rate of structured electrode made using ceramic structuring tool. Figure (b) shows relative discharge capacity and coulombic efficiency against C-rate of structured electrode made using metal structuring tool.

.

Comparing the unstructured electrodes to the structured electrodes demonstrates significant differences in rate capability performance between the two for the thinner electrodes. The structured electrodes exhibit slightly lower rate capability performance at very low C-rates. This could be due to wetting challenges with using lignin as binder rather than purely due to structures. Another reason for this difference could be due to imperfect structures on the electrodes that can cause multiple issues. This will be discussed in further detail in the next section when comparing the thinner electrodes with the thicker electrodes.

At C-rates exceeding 1C there is a clear distinction in rate capability performance between unstructured electrodes and structured electrodes. At medium C-rates, between 1 and 2 C, the reduction in rate capability slows down in structured electrodes versus in unstructured electrodes where there is a rapid reduction. At higher C-rates, exceeding 2C, the reduction in rate capability tapers off signifi-

cantly in structured electrodes compared to the larger reduction for unstructured electrodes. This is true for the structures produced using the metal blade and the ceramic blade structuring tools.

4.2.2 150 μm electrodes

The thicker electrodes were 150 μm thick and subjected to the same testing conditions as the thinner electrodes.Figure 4.2.3a shows the specific discharge capacity (mAh/g) against the C-rate which has undergone 38 cycles at incrementally increasing C-rates. Coulombic efficiency is also included in the figure. Similar to the thinner electrodes, Figure 4.2.3a and Figure 4.2.3b show a considerable reduction in capacity retention as C-rate increases. Once again, this is particularly apparent when observing the transition from low C-rates towards higher C-rates. The data for the thicker electrodes was also plotted as relative specific discharge capacity against C-rate as seen in Figure 4.2.3b.

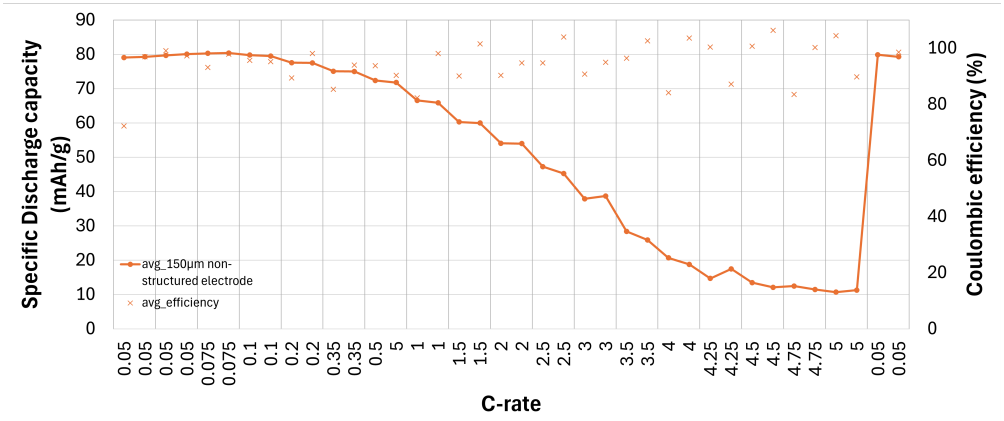

(a) Specific discharge capacity of 150 μm unstructured electrode

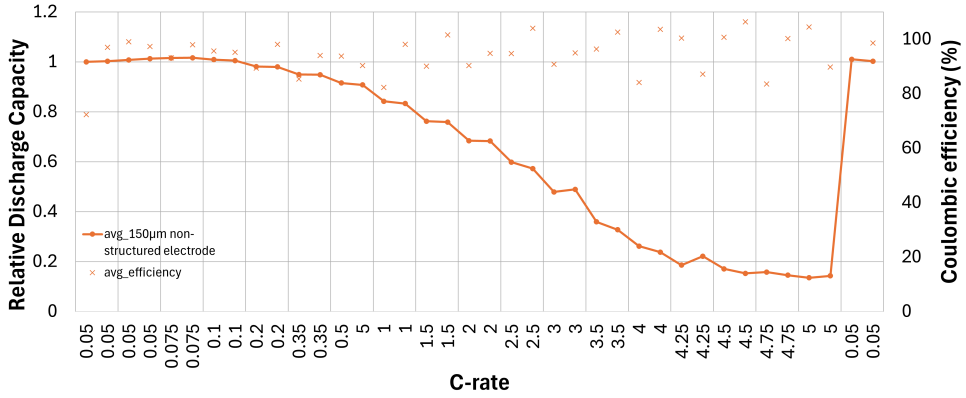

(b) Relative discharge capacity of 150 μm unstructured electrode

Figure 4.2.3: Average rate performance of unstructured 150 μm thick electrodes. Figure (a) shows specific discharge capacity and coulombic efficiency against C-rate. Figure (b) shows relative discharge capacity and coulombic efficiency against C-rate.

Figure 4.2.4a shows the relative specific discharge capacity of a structured electrode using the ceramic blades (CB) used for structuring. Unlike the thinner electrodes, the CB structured electrodes do not show a noticeable difference in capacity retention compared to the unstructured electrode shown in Figure 4.2.3b.If anything, the capacity retention seems slightly worse than the unstructured electrode. This is most likely due to poor corrugation depth on the surface of the electrodes. The ceramic blades had difficulty penetration deeply enough to create actual corrugated structures in most of the thick electrodes. Instead of acquiring uniform corrugations on the surface of the electrode, only non-uniform indentations were made. This is reflected in the data where imperfect structures caused lower rate capacity retention at high C-rates, exceeding 2.5C, as shown in Figure 4.2.4a compared to Figure 4.2.3b.

Figure 4.2.4b shows the structured electrode using the metal blades (CB). Unlike the ceramic blades, the metal blades did not have issues penetrating deeply enough into the electrode surface and thus achieved results consistent with the thinner structured electrodes.Figure 4.2.4b illustrates this as the relative specific discharge capacity reduces from 37.5% down to 24% at high C-rates ranging from 3C to 5C. This is an improvement in capacity retention compared to Figure 4.2.3b where the relative specific discharge capacity drops from around 35% to down 12.5% at the higher C-rates ranging from 3C to 5C.

At lower C-rates, the thicker electrodes do perform slightly worse than the unstructured electrodes in terms of capacity retention. This could be due to imperfect structures on the surface. The lack of uniformity could cause disturbances to the kinetics in the Li-ion cell. Another issue that could be the culprit is the removal of active material during structuring, lowering the overall capacity.

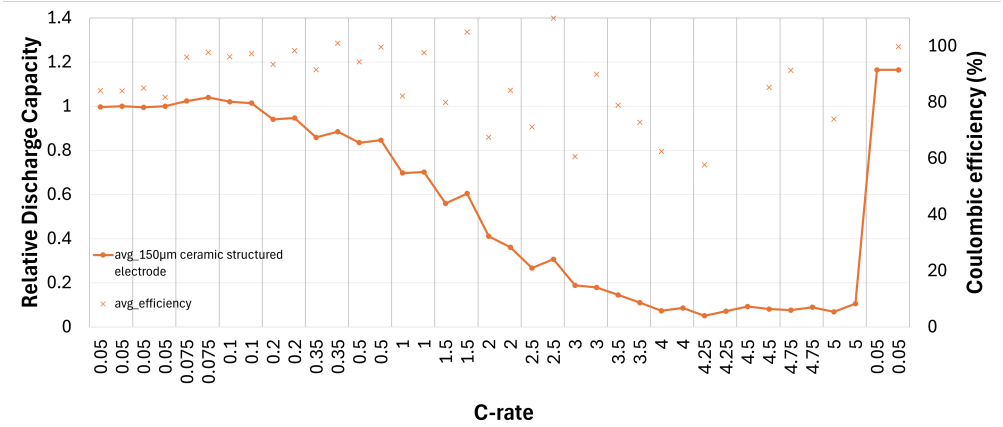

(a) Relative discharge capacity of 150 μm ceramic structured electrode

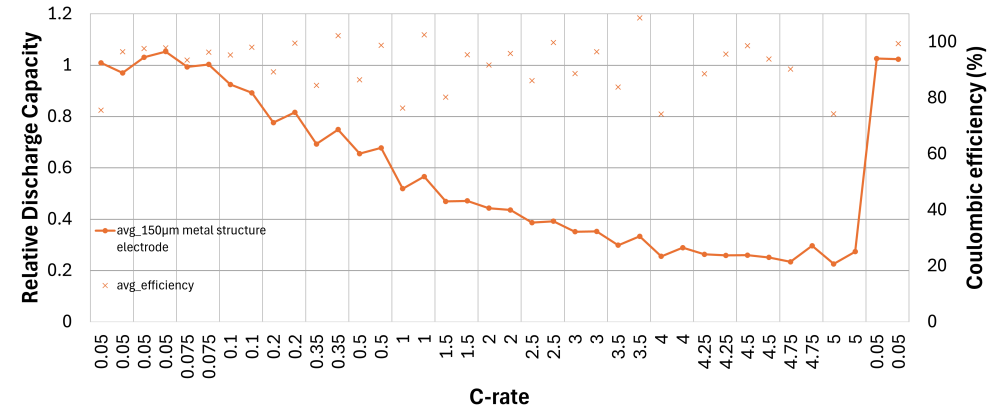

(b) Relative discharge capacity of 150 μm metal structured electrode

Figure 4.2.4: Average rate performance of structured 150 μm thick electrodes. Figure (a) shows relative discharge capacity and coulombic efficiency against C-rate of structured electrode made using ceramic structuring tool. Figure (b) shows relative discharge capacity and coulombic efficiency against C-rate of structured electrode made using metal structuring tool.

.

Analysing and comparing the results from the unstructured and structured electrodes, there are a few key takeaways. First, the structuring was imperfect, i.e. no two structures were exactly the same. This was due to the limitations of mechanical structuring in a small scale laboratory environment. There will always be discrepancies in the application of the structuring tools to the surface of the electrode even with a standard operating procedure. The lack of uniformity and the high probability of removal of active material due to the structures meant that there was a high likelihood the capacity would be affected. In spite of this, clear trends can be observed when comparing the structured electrodes to the unstructured ones. The structured electrodes showed a significant improvement in rate capacity retention at high C-rates. The thinner structured electrodes also showed a slight improvement in rate capacity retention at C-rates ranging from 1C to 3C, whereas the thicker structured electrodes showed a slight decrease in rate capacity retention at the aforementioned medium C-rates.

Additionally, a different potential effect of imperfect structuring is that it could lead to excessive removal of active material by penetrating through the whole electrode, even completely through to the current collector in some areas. This is supported by the data when comparing the thinner to the thick electrodes and could be seen on some of the thinner electrodes. The thicker structured electrodes do not have the same decrease in capacity retention at low c-rates which could indicate potentially more active material was removed.

Another interesting takeaway is the apparent higher fluctuation in values for the structured electrodes. A likely reason for this could be the lack of uniformity in the structures. Some electrodes probably had more uniform structures facilitating faster Lithium ion transport whereas some other electrodes will have had less uniform structures causing a wider variation in results compared to the unstructured electrodes.

Lastly, observing the capacity at higher C-rates, it is clear that thinner electrodes perform better at high C-rates than thicker electrodes. This is presumably due to the thicker electrodes having longer ion and electron paths compared to thinner electrodes. The shorter ion and electron paths lead to improved rate capacity retention at high C-rates. Corrugations exacerbate this phenomena by further increasing rate capability at high C-rates [6].

4.3 Mass transport analysis

To understand why structured electrodes have improved rate capability at higher C-rates, mass transport of lithium ions must be examined. Lithium ion transport plays a pivotal role in determining capacity retention, especially at high C-rates. The following section presents the mass transport results while discussing the major takeaways. The effective mass transport coefficient was obtained from the concentration over-potentials for electrodes of different thicknesses and structures. Since no two manufactured electrodes are the same, the effective mass transfer coefficients include a calculated standard deviation to account for discrepancies in the production of different electrodes.

4.3.1 Reaction and concentration overpotentials

Figure 4.3.1 displays the concentration over-potential plotted against the current density for the relevant SoCs. The effective mass transport coefficient is found at the limiting current density, when the concentration at the surface is zero. This is illustrated by the curve-fits of the data in Figure 4.3.1a and Figure 4.3.1b. The results suggest there is not a significant difference in concentration over-potential between the thinner and thicker electrodes. Using the results shown in Figure 4.3.1

the effective mass transfer coefficients can be calculated and are presented in the following subsection.

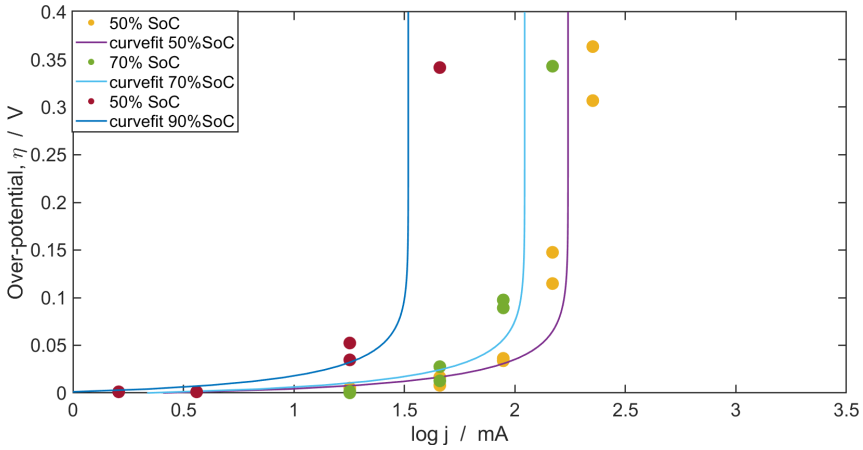

(a) η vs. log j plot of unstructured 100 μm thick electrode.

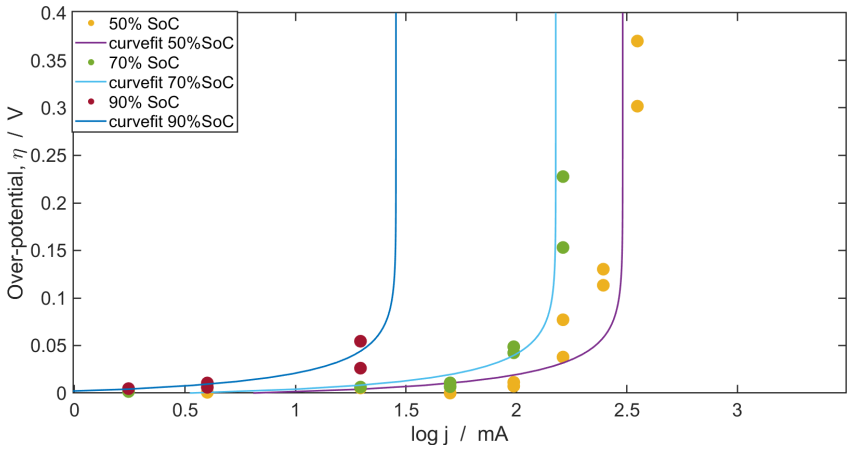

(b) η vs. log j plot of unstructured 150 μm thick electrode.

Figure 4.3.1: The concentration over-potential plotted against the current density at 50%, 70% and 90% state of charge, including a curve-fit to determine limiting current density, for: (a) a 100 μm thick unstructured electrode and (b) a 150 μm thick unstructured electrode.

4.3.2 Effective mass transport coefficient

100 μm electrodes

The initial results shown are for the 100 μm thick electrodes. The analysis presents the effective mass transfer coefficient, h_m, at various state of charges. The SoCs chosen were 50, 70 and 90 percent. These were chosen to get a good spread of the values of h_m to represent the change of the effective mass transfer coefficient under discharge of a battery.

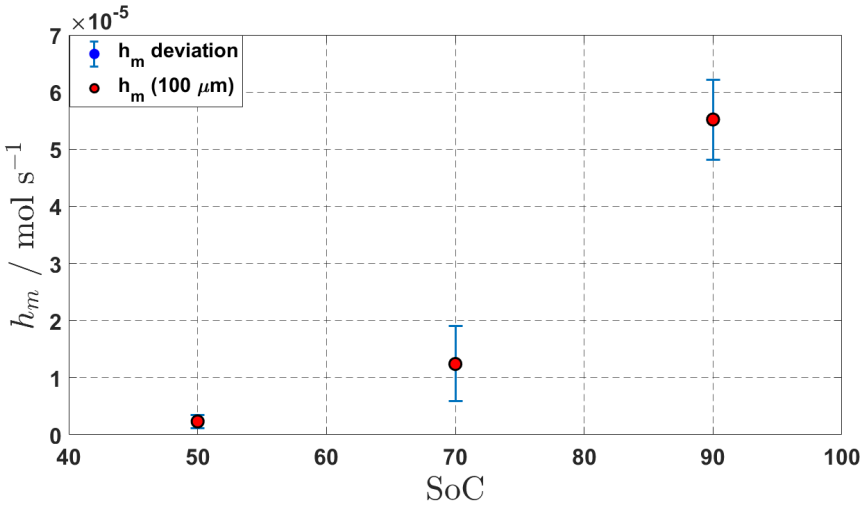

Figure 4.3.2: Mass transport coefficient plotted against state of charge for unstructured electrodes of 100 μm thickness.

Figure 4.3.2 shows the effective mass transfer coefficient, h_m, for an 100 μm thick unstructured electrode against the nominal state of charge, SoC, of the battery. As the state of charge increases, h_m also increases. At higher SoCs there is more uncertainty in h_m which is shown by the larger error bars. This uncertainty is most likely due to increased noise as stationary diffusion regions haven't developed yet. These results are used as the baseline to compare against the structured electrodes of a similar thickness and observe the differences in effective mass transfer coefficients due to corrugations.

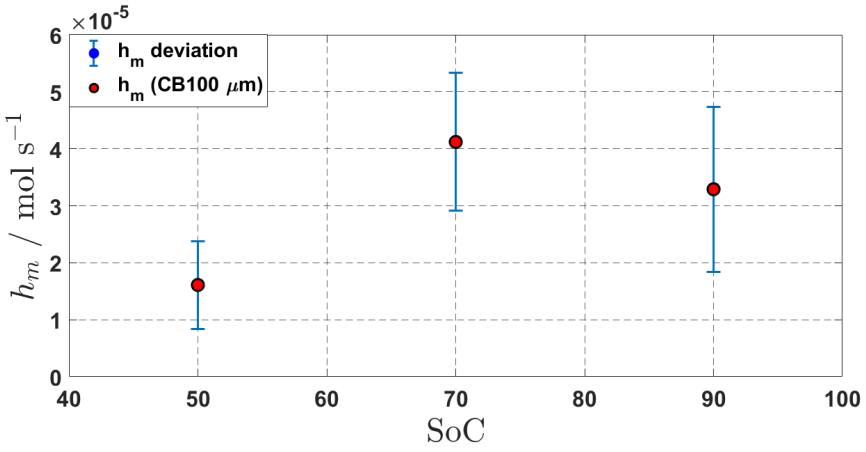

Figure 4.3.3: Mass transport coefficient plotted against state of charge for structured (CB) electrodes of 100 μm thickness.

The next figure,Figure 4.3.3 shows the effective mass transfer coefficient, h_m, for an 100 μm thick structured (CB) electrode against the nominal state of charge, SoC, of the battery. Once again, as the state of charge increases, h_m also increases. At 50 % and 70% SoC, the effective mass transfer coefficient is higher than the unstructured electrode of the same thickness. This is consistent with the theory,

that corrugations and surface structures cause faster Li ion transportation and increased diffusivity, which correlates to a higher effective mass transfer coefficient. The outlier here is the effective mass transfer coefficient at 90% SoC. The h_m is lower than the corresponding value for the unstructured electrode of a similar thickness. This could be due to a variety of reasons. As mentioned earlier, there is more uncertainty in h_m values at high state of charges due to a higher degree of noise, sensor errors or model inaccuracies in characterisation of lithium ion batteries [63].

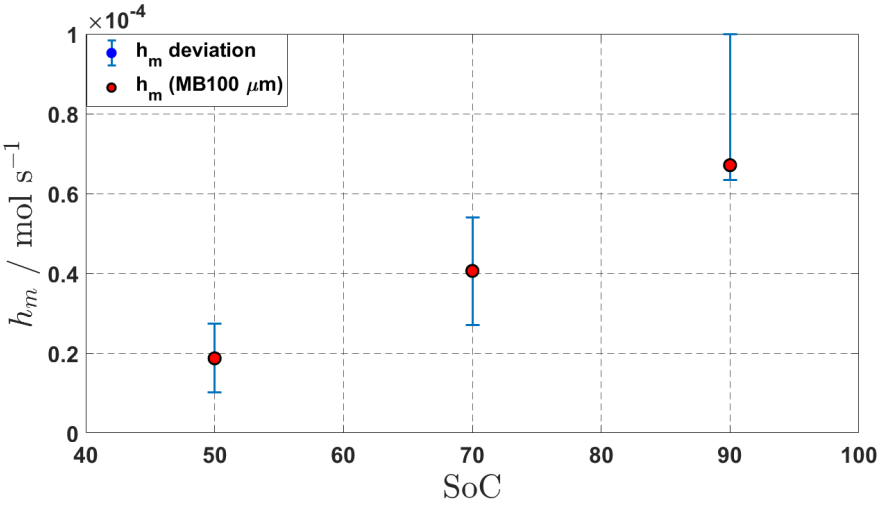

Figure 4.3.4: Mass transport coefficient plotted against state of charge for structured (MB) electrodes of 100 μm thickness.

Figure 4.3.4 shows the effective mass transfer coefficient, h_m, for an 100 μm thick structured (MB) electrode against the nominal state of charge, SoC, of the battery. The figure shows an increase in h_m as SoC increases. Similarly to the other electrodes, the variance in h_m is larger at higher SoCs as can clearly be seen by the large variation shown at 90% SoC. Comparing the structured electrodes to the unstructured strengthens the premise of a higher effective mass transfer coefficient for structured electrodes as opposed to unstructured electrodes.

150 μm electrodes

The following figures present the same results as the previous sections, but for the thicker electrodes. The electrodes were 150 μm thick. As before the analysis presents the effective mass transfer coefficient, h_m, at 50 %, 70% and 90% charge.

The first figure, Figure 4.3.5, shows the effective mass transfer coefficient at 50%, 70% and 90% state of charge for an unstructured electrode. Similarly to the thinner electrodes, h_m increases with state of charge.

Figure 4.3.6 shows a considerable increase in effective mass transfer coefficient for an 150 μm thick structured (CB) electrode compared to an unstructured electrode of a similar thickness. The increase of the effective mass transport coefficient

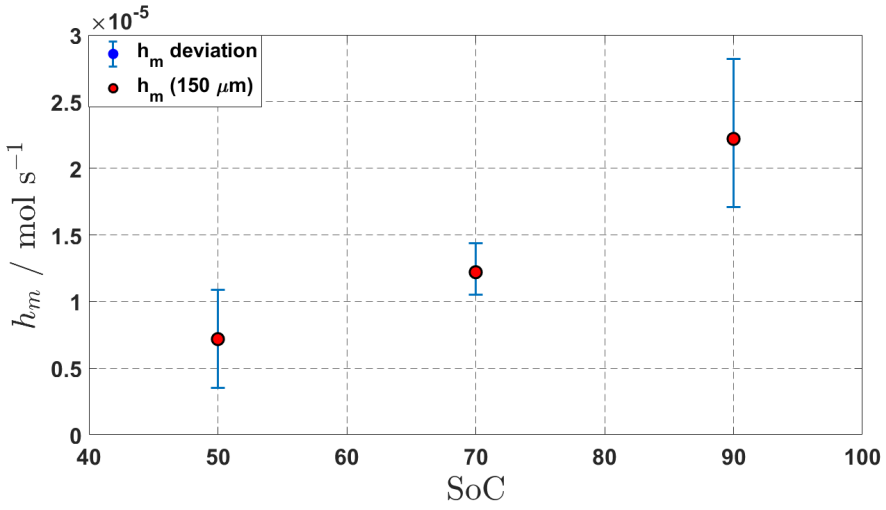

Figure 4.3.5: Mass transport coefficient plotted against state of charge for unstructured electrodes of 150 μm thickness.

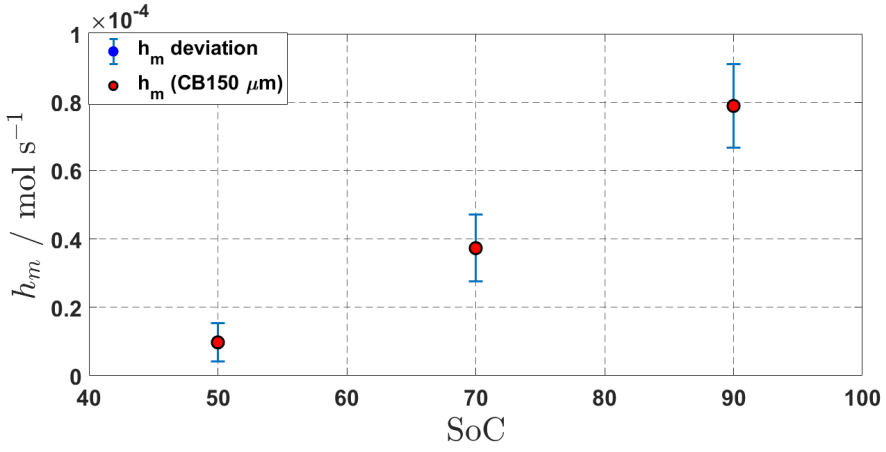

Figure 4.3.6: Mass transport coefficient plotted against state of charge for structured (CB) electrodes of 150 μm thickness.

is considerable and strengthens the hypothesis discussed earlier about the positive effect of structures on reducing mass transport limitations.

The last figure, Figure 4.3.7, shows a noticeable increase in effective mass transfer coefficient for an 150 μm thick structured (MB) electrode compared to an unstructured electrode of a similar thickness. Though the increase is less than the other structured electrodes of a similar thickness, the difference is enough to confirm a distinct increase in the effective mass transfer coefficient.

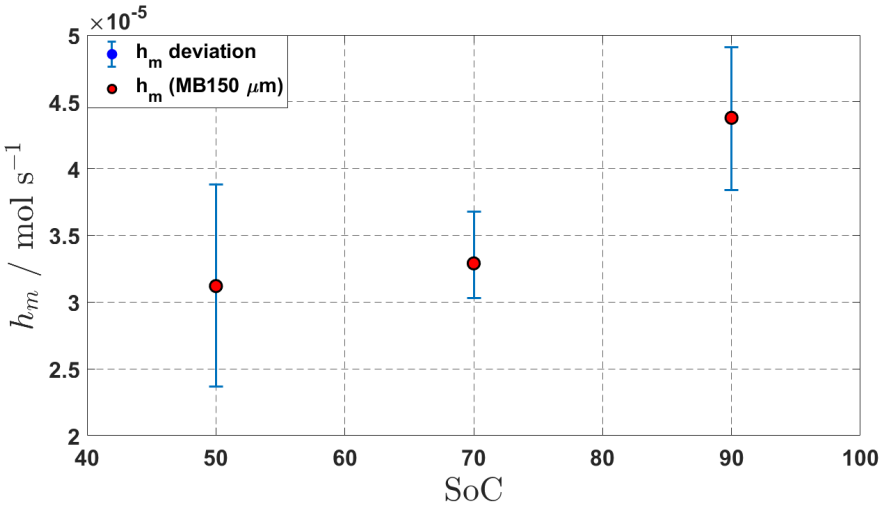

Figure 4.3.7: Mass transport coefficient plotted against state of charge for structured (MB) electrodes of 150 μm thickness.

4.3.3 Effective mass transfer coefficient comparison

It is safe to conclude that the effective mass transfer coefficient increases with increasing state of charge. Additionally, the results have shown that the effective mass transfer coefficient is higher for structured electrodes as opposed to unstructured electrodes of the same type. Comparing the effective mass transfer and the relative increase of h_m between thicknesses is an interesting matter to analyse. The following graphs compare the effective mass transfer coefficients of the different types of electrodes tested during this study to each other at their respective state of charge.

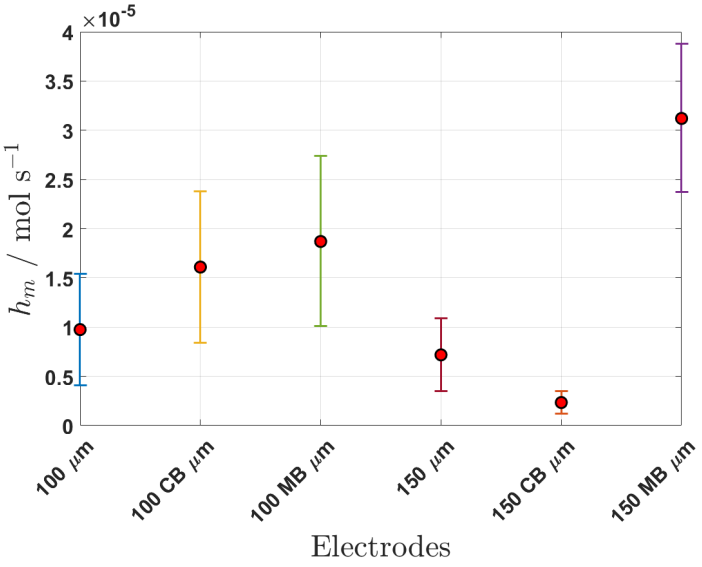

Figure 4.3.8: Figure comparing the effective mass transport coefficient for different types of electrodes produced at 50% state of charge.

Figure 4.3.8 presents the effective mass transfer coefficients of the different

electrode types produced for testing at 50% state of charge. The electrode types are listed on the x-axis, with the first three being the thinner electrodes (100 μm) and the latter three being the thicker electrodes (150 μm). The electrode types are sorted as follows: unstructured, followed by structured electrodes using the ceramic blade structuring tool (CB), and then the structured electrodes using the metallic blade structuring tool (MB). An interesting element to note is that the thicker unstructured electrodes have a higher effective mass transfer coefficient than the thinner ones. When comparing the "CB" structured electrodes, the thinner electrode has a significantly higher relative increase than the thicker electrode. This could be due to the general difficulty in structuring the thicker electrodes using the ceramic blade structuring tool.

A final observation that should be noted is the large increase in h_m for the "MB" structured electrodes. Especially the thicker electrode had a substantial increase in effective mass transfer coefficient. For both electrode types, structuring had a positive effect on mass transport behaviour when half the capacity had already been discharged.

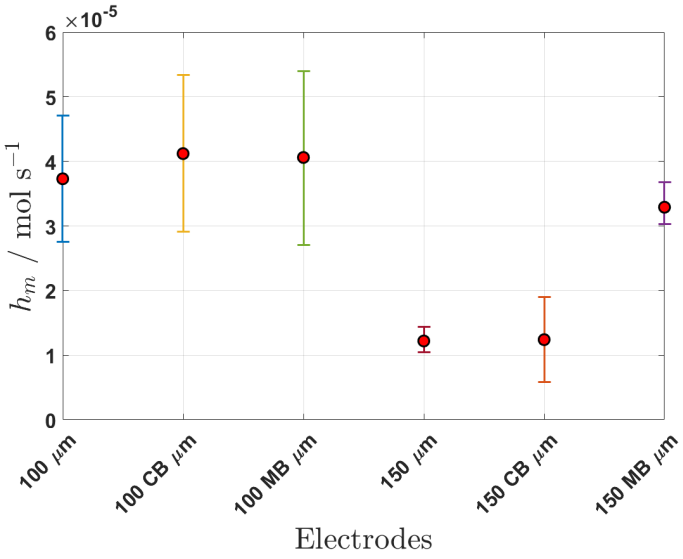

Figure 4.3.9: Figure comparing the effective mass transport coefficient for different types of electrodes produced at 70% state of charge.

Figure 4.3.9 shows the effective mass transfer coefficients of the different electrode types at 70% state of charge. When the batteries reached 70% state of charge, there is a considerable increase in effective mass transfer coefficient going from unstructured to structured electrodes. A peculiar observation is that the thinner electrodes had a similar relative increase in mass transport compared to the thicker electrodes. The thinner electrodes even have slightly higher h_m values suggesting that the thinner electrodes have marginally better mass transport kinetics than the thicker electrodes.

As discussed earlier, the results at high state of charge aren't quite as reliable as the ones at lower SoC due to the larger amount of uncertainty. This

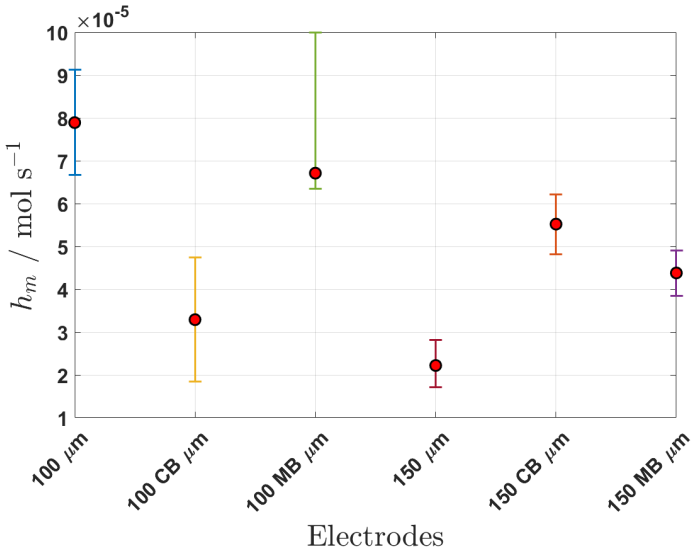

Figure 4.3.10: Figure comparing the effective mass transport coefficient for different types of electrodes produced at 90% state of charge.

is reflected in Figure 4.3.10 which shows the results of the effective mass transfer coefficients of the different electrode types at 90% state of charge. The thicker electrodes behave as expected with the structured electrodes with an effective mass transfer coefficient exceeding the unstructured electrodes. Conversely, the thinner electrodes exhibit significant fluctuations, with one type of structured electrode displaying a lower effective mass transfer coefficient compared to the unstructured electrodes. It is difficult to ascertain if this is uncertainty deriving from the electrode structure, the limited wetting time, the measuring instrument or some other reason. Therefore it is difficult to to draw absolute conclusions from Figure 4.3.10.

Some interesting observations can be made from this mass transport analysis. In general the ceramic blade (CB) structuring tool gave mixed results and wasn't as reliable as the metal blade (MB) structuring tool when creating line corrugations in the material. This was also observed during the use of scanning electron microscopy on the electrodes. Overall, the metal blade structuring tool gave more uniform and consistent structuring but also carried the increased risk of removing more active material than the ceramic blade structuring tool.

The mass transport analysis corroborates the hypothesis that increased mass transport in electrodes corresponds to better rate capacity retention. Corrugations and structures on the surface of the electrodes provide a noticeable effect on the effective mass transfer coefficient, increasing h_m significantly compared to unstructured electrodes.

The thinner electrodes generally provided more consistent results, except at high states of charge. At high SoC, there was a larger degree of uncertainty when

observing the effective mass transfer coefficient. The thinner electrodes were shown to have better mass transport than the thicker electrodes. A post-mortem analysis could provide insight on the state of the corrugations and structures after cycling. This could give an indication whether structures were degraded and if that related to uncertainty in the effective mass transport coefficient results.

CHAPTER

FIVE

CONCLUSIONS

The rate capacity retention analysis displayed clear trends when comparing the structured electrodes to those without structures. The structured electrodes showed a considerable improvement in rate capacity retention at high C-rates, ranging from 3.5C to 5C. Additionally, the thinner structured electrodes outperformed the thicker structured electrodes at medium C-rates, ranging from 1C to 3C.

The mass transport analysis showed that increased mass transport in electrodes corresponds to better rate capacity retention. Corrugations and structures on the surface of the electrodes provided a significant effect on the effective mass transfer coefficient, increasing the effective mass transfer coefficient significantly, by up to 5 times, compared to unstructured electrodes.

The thinner electrodes generally provided more consistent results, except at high states of charge. At high SoC, there was a larger degree of uncertainty when observing the effective mass transfer coefficient, likely due to increased noise as the stationary diffusion regions had not yet developed. The thinner electrodes were shown to generally have a higher effective mass transfer coefficient than the thicker electrodes.

Structuring of the electrodes was found to be difficult to keep completely consistent as there was a certain degree of variation in the uniformity of the corrugations in the structured electrodes. The thinner electrodes were more likely to suffer from excessive removal of material than the thicker electrodes, whereas the thicker electrodes were more likely to suffer from insufficient penetration by the corrugations into the surface of the electrode. This caused some fluctuation in the results but not excessively so. As expected there was simply a wider variation in results for structured electrodes compared to unstructured electrodes.

CHAPTER

SIX

FURTHER WORK

Building on this work could be done by experimenting with the density of corrugations on the electrode. More variety in the distance between corrugations would be an interesting analysis to perform. To see if there is a point of diminishing returns where the increase in mass transport becomes so small that the effect on the performance of the battery becomes negligible. Examining what the trade-off between tightly packed corrugations on the surface of the electrode and increased thickness would be. As the corrugations become more tightly packed, the less material is available. The opposite could also be interesting, how far can the structures be placed from each other and how would that effect the mass transport properties and capacity retention.

Further work on the three electrode setup to analyse the overpotential contributions from the anode and cathode individually using a reference electrode could better determine where the electrochemical response originates from during cycling of the battery. This could provide more valuable insight into the relationship between rate capacity retention and the effective mass transfer coefficient for a structured electrode. Using electrochemical impedance spectroscopy, EIS, to investigate the impedance and provide information on the diffusion processes in a structured electrode.

Another interesting continuation of this work could be to examine the effect of structuring on ageing. Whether structuring improves ageing characteristics over multiple cycles or if the structures deteriorate and negatively impact the battery performance.

REFERENCES

[1] Ronan Njøs Dunne. *Increasing energy density with improved transport properties in lithium-ion batteries*. NTNU. Unpublished. Dec. 2023.

[2] *THE 17 GOALS | Sustainable Development*. [Online; accessed 12. Oct. 2023]. Oct. 2023. URL: https://sdgs.un.org/goals#history.

[3] United Nations. *Support Sustainable Development and Climate Action | United Nations*. Oct. 2023. URL: https://www.un.org/en/our-work/support-sustainable-development-and-climate-action.

[4] Yangtao Liu et al. "Current and future lithium-ion battery manufacturing". In: *iScience* 24.4 (Apr. 2021), p. 102332. ISSN: 2589-0042. DOI: 10.1016/j.isci.2021.102332.

[5] Odne Stokke Burheim. "Chapter 7 - Secondary Batteries". In: *Engineering Energy Storage*. Cambridge, MA, USA: Academic Press, Jan. 2017, pp. 111–145. ISBN: 978-0-12-814100-7. DOI: 10.1016/B978-0-12-814100-7.00007-9.

[6] Silje Nornes Bryntesen et al. "Opportunities for the State-of-the-Art Production of LIB Electrodes—A Review". In: *Energies* 14.5 (Mar. 2021), p. 1406. ISSN: 1996-1073. DOI: 10.3390/en14051406.

[7] Arno Kwade1, Markus Noeske1, Michael Grube, Jutta Hesselbach and Sabrina Zellmer, "Milling within Energy Storage Industry ",16th European Symposium on Comminution Classification (ESCC 2019). Aug. 2019. URL: https://eprints.whiterose.ac.uk/150219/1/ESCC2019%20-%20Book%20of%20Extended%20Abstracts%20-%20Provisional%20Copy%20.pdf.

[8] Lena Spitthoff, Paul R. Shearing, and Odne Stokke Burheim. "Temperature, Ageing and Thermal Management of Lithium-Ion Batteries". In: *Energies* 14.5 (Feb. 2021), p. 1248. ISSN: 1996-1073. DOI: 10.3390/en14051248.

[9] Muammer Kaya. "State-of-the-art lithium-ion battery recycling technologies". In: *Circular Economy* 1 (Oct. 2022). ISSN: 2773-1677. DOI: 10.1016/j.cec.2022.100015.

[10] Robert D. Minter et al. "JoVE". In: *JoVE (Journal of Visualized Experiments)* 135 (May 2018), e57735. ISSN: 1940-087X. DOI: 10.3791/57735.

[11] Dennis W. Dees, Andrew N. Jansen, and Daniel P. Abraham. "Theoretical examination of reference electrodes for lithium-ion cells". In: *J. Power Sources* 174.2 (Dec. 2007), pp. 1001–1006. ISSN: 0378-7753. DOI: 10.1016/j.jpowsour.2007.06.128.

[12] Sophie Solchenbach et al. "A Gold Micro-Reference Electrode for Impedance and Potential Measurements in Lithium Ion Batteries". In: *Journal of The Electrochemical Society* 163 (10 2016), A2265–A2272. ISSN: 0013-4651. DOI: 10.1149/2.0581610jes.

[13] Andreas Karg et al. "An Integrated, Exchangeable Three-Electrode Electrochemical Setup for AFM-Based Scanning Electrochemical Microscopy". In: *Sensors* 23.11 (May 2023), p. 5228. ISSN: 1424-8220. DOI: 10.3390/s23115228.

[14] Werner Schlemmer et al. "Polysaccharides for sustainable energy storage – A review". In: *Carbohydr. Polym.* 265 (Aug. 2021), p. 118063. ISSN: 0144-8617. DOI: 10.1016/j.carbpol.2021.118063.

[15] Shuai Liu et al. "Understanding the Conductive Carbon Additive on Electrode/Electrolyte Interface Formation in Lithium-Ion Batteries via in situ Scanning Electrochemical Microscopy". In: *Front. Chem.* 8 (Feb. 2020), p. 524049. ISSN: 2296-2646. DOI: 10.3389/fchem.2020.00114.

[16] Niranjanmurthi Lingappan, Lingxi Kong, and Michael Pecht. "The significance of aqueous binders in lithium-ion batteries". In: *Renewable Sustainable Energy Rev.* 147 (Sept. 2021), p. 111227. ISSN: 1364-0321. DOI: 10.1016/j.rser.2021.111227.

[17] A. Du Pasquier et al. "Differential Scanning Calorimetry Study of the Reactivity of Carbon Anodes in Plastic Li-Ion Batteries". In: *J. Electrochem. Soc.* 145.2 (Feb. 1998), p. 472. ISSN: 1945-7111. DOI: 10.1149/1.1838287.

[18] Hossein Maleki et al. "Thermal Stability Studies of Binder Materials in Anodes for Lithium-Ion Batteries". In: *J. Electrochem. Soc.* 147.12 (Dec. 2000), p. 4470. ISSN: 1945-7111. DOI: 10.1149/1.1394088.

[19] Huiran Lu et al. "Lignin as a Binder Material for Eco-Friendly Li-Ion Batteries". In: *Materials* 9.3 (Feb. 2016), p. 127. ISSN: 1996-1944. DOI: 10.3390/ma9030127.

[20] John T. Warner. *Lithium-Ion Battery Chemistries*. Walthm, MA, USA: Elsevier, 2019. ISBN: 978-0-12-814778-8. DOI: 10.1016/C2017-0-02140-7.

[21] Ghassan Zubi et al. "The lithium-ion battery: State of the art and future perspectives". In: *Renewable Sustainable Energy Rev.* 89 (June 2018), pp. 292–308. ISSN: 1364-0321. DOI: 10.1016/j.rser.2018.03.002.

[22] Shankar Aryal et al. "Roles of Mn and Co in Ni-rich layered oxide cathodes synthesized utilizing a Taylor Vortex Reactor". In: *Electrochim. Acta* 391 (Sept. 2021), p. 138929. ISSN: 0013-4686. DOI: 10.1016/j.electacta.2021.138929.

[23] Yu Miao et al. "Current Li-Ion Battery Technologies in Electric Vehicles and Opportunities for Advancements". In: *Energies* 12.6 (Mar. 2019), p. 1074. ISSN: 1996-1073. DOI: 10.3390/en12061074.

[24] Naoki Nitta et al. “Li-ion battery materials: present and future”. In: *Mater. Today* 18.5 (June 2015), pp. 252–264. ISSN: 1369-7021. DOI: 10.1016/j.mattod.2014.10.040.

[25] J. R. Dahn et al. “Thermal stability of LixCoO2, LixNiO2 and λ-MnO2 and consequences for the safety of Li-ion cells”. In: *Solid State Ionics* 69.3 (Aug. 1994), pp. 265–270. ISSN: 0167-2738. DOI: 10.1016/0167-2738(94)90415-4.

[26] Erying Zhao et al. “A low-cost and eco-friendly network binder coupling stiffness and softness for high-performance Li-ion batteries”. In: *Electrochim. Acta* 387 (Aug. 2021), p. 138491. ISSN: 0013-4686. DOI: 10.1016/j.electacta.2021.138491.

[27] “Lithium-Secondary Cell: Sources of Risks and Their Effects”. In: *Electrochemical Power Sources: Fundamentals, Systems, and Applications*. Walthm, MA, USA: Elsevier, Jan. 2019, pp. 143–266. ISBN: 978-0-444-63777-2. DOI: 10.1016/B978-0-444-63777-2.00007-4.

[28] *Carbon-Based Anode - an overview | ScienceDirect Topics*. [Online; accessed 3. Nov. 2023]. Jan. 2023. DOI: 10.1016/B978-0-444-64017-8.00016-6.

[29] P. U. Nzereogu et al. “Anode materials for lithium-ion batteries: A review”. In: *Applied Surface Science Advances* 9 (June 2022), p. 100233. ISSN: 2666-5239. DOI: 10.1016/j.apsadv.2022.100233.

[30] Mario Wachtler, Martin Winter, and Jürgen O. Besenhard. “Anodic materials for rechargeable Li-batteries”. In: *J. Power Sources* 105.2 (Mar. 2002), pp. 151–160. ISSN: 0378-7753. DOI: 10.1016/S0378-7753(01)00934-X.

[31] Jiale Xing et al. “A Review of Nonaqueous Electrolytes, Binders, and Separators for Lithium-Ion Batteries”. In: *Electrochem. Energy Rev.* 5.4 (Dec. 2022), pp. 1–34. ISSN: 2520-8136. DOI: 10.1007/s41918-022-00131-z.

[32] Candice F. J. Francis, Ilias L. Kyratzis, and Adam S. Best. “Lithium-Ion Battery Separators for Ionic-Liquid Electrolytes: A Review”. In: *Adv. Mater.* 32.18 (May 2020), p. 1904205. ISSN: 0935-9648. DOI: 10.1002/adma.201904205.

[33] Valadoula Deimede and Costas Elmasides. “Separators for Lithium-Ion Batteries: A Review on the Production Processes and Recent Developments”. In: *Energy Technology* 3.5 (May 2015), pp. 453–468. ISSN: 2194-4288. DOI: 10.1002/ente.201402215.

[34] Chris Yuan et al. “Manufacturing energy analysis of lithium ion battery pack for electric vehicles”. In: *CIRP Ann.* 66.1 (Jan. 2017), pp. 53–56. ISSN: 0007-8506. DOI: 10.1016/j.cirp.2017.04.109.

[35] Silje Nornes Bryntesen. “Production Strategies for Sustainable LIB Cathodes with Enhanced Rate Capability and Energy Density”. PhD thesis. Norway: NTNU, 2023. ISBN: 978-82-326-5692-9. URL: https://ntnuopen.ntnu.no/ntnu-xmlui/handle/11250/3062881.

[36] Arno Kwade et al. “Current status and challenges for automotive battery production technologies”. In: *Nat. Energy* 3 (Apr. 2018), pp. 290–300. ISSN: 2058-7546. DOI: 10.1038/s41560-018-0130-3.

[37] Anh Vu, Yuqiang Qian, and Andreas Stein. "Porous Electrode Materials for Lithium-Ion Batteries – How to Prepare Them and What Makes Them Special". In: *Adv. Energy Mater.* 2.9 (Sept. 2012), pp. 1056–1085. ISSN: 1614-6832. DOI: 10.1002/aenm.201200320.

[38] Yudi Kuang et al. "Thick Electrode Batteries: Principles, Opportunities, and Challenges". In: *Adv. Energy Mater.* 9.33 (Sept. 2019), p. 1901457. ISSN: 1614-6832. DOI: 10.1002/aenm.201901457.

[39] Carl D. Reynolds et al. "A review of metrology in lithium-ion electrode coating processes". In: *Mater. Des.* 209 (Nov. 2021), p. 109971. ISSN: 0264-1275. DOI: 10.1016/j.matdes.2021.109971.

[40] Pengcheng Zhu, Peter R. Slater, and Emma Kendrick. "Insights into architecture, design and manufacture of electrodes for lithium-ion batteries". In: *Mater. Des.* 223 (Nov. 2022), p. 111208. ISSN: 0264-1275. DOI: 10.1016/j.matdes.2022.111208.

[41] Jianlin Li et al. "From Materials to Cell: State-of-the-Art and Prospective Technologies for Lithium-Ion Battery Electrode Processing". In: *Chem. Rev.* 122.1 (Jan. 2022), pp. 903–956. ISSN: 0009-2665. DOI: 10.1021/acs.chemrev.1c00565.

[42] Antje Schilling et al. "Analyzing Bending Stresses on Lithium-Ion Battery Cathodes induced by the Assembly Process". In: *Energy Technology* 4 (Aug. 2016). DOI: 10.1002/ente.201600131.

[43] Mei Cai. "Best practices in lithium battery cell preparation and evaluation". In: *Research Communities by Springer Nature* (Jan. 2023). URL: https://communities.springernature.com/posts/best-practices-in-lithium-battery-cell-preparation-and-evaluation.

[44] Roman Nölle et al. "A reality check and tutorial on electrochemical characterization of battery cell materials: How to choose the appropriate cell setup". In: *Mater. Today* 32 (Jan. 2020), pp. 131–146. ISSN: 1369-7021. DOI: 10.1016/j.mattod.2019.07.002.

[45] Jiale Xie et al. "Puzzles and confusions in supercapacitor and battery: Theory and solutions". In: *J. Power Sources* 401 (Oct. 2018), pp. 213–223. ISSN: 0378-7753. DOI: 10.1016/j.jpowsour.2018.08.090.

[46] W. Wang et al. "Electrochemical cells for medium- and large-scale energy storage: fundamentals". In: *Advances in Batteries for Medium and Large-Scale Energy Storage*. Buckingham, England, UK: Woodhead Publishing, Jan. 2015, pp. 3–28. ISBN: 978-1-78242-013-2. DOI: 10.1016/B978-1-78242-013-2.00001-7.

[47] Edmund J. F. Dickinson and Andrew J. Wain. "The Butler-Volmer equation in electrochemical theory: Origins, value, and practical application". In: *J. Electroanal. Chem.* 872 (Sept. 2020), p. 114145. ISSN: 1572-6657. DOI: 10.1016/j.jelechem.2020.114145.

[48] Marcelo Carmo and Detlef Stolten. "Energy Storage Using Hydrogen Produced From Excess Renewable Electricity: Power to Hydrogen". In: *Science and Engineering of Hydrogen-Based Energy Technologies*. Cambridge, MA, USA: Academic Press, Jan. 2019, pp. 165–199. ISBN: 978-0-12-814251-6. DOI: 10.1016/B978-0-12-814251-6.00004-6.

[49] David McNulty et al. "A review of Li-ion batteries for autonomous mobile robots: Perspectives and outlook for the future". In: *J. Power Sources* 545 (Oct. 2022), p. 231943. ISSN: 0378-7753. DOI: 10.1016/j.jpowsour.2022.231943.

[50] Jacqueline S. Edge et al. "Lithium ion battery degradation: what you need to know". In: *Phys. Chem. Chem. Phys.* 23.14 (2021), pp. 8200–8221. DOI: 10.1039/D1CP00359C.

[51] Panpan Hu et al. "Joint State of Charge (SOC) and State of Health (SOH) Estimation for Lithium-Ion Batteries Packs of Electric Vehicles Based on NSSR-LSTM Neural Network". In: *Energies* 16.14 (July 2023), p. 5313. ISSN: 1996-1073. DOI: 10.3390/en16145313.

[52] *Encyclopedia of Electrochemical Power Sources*. [Online; accessed 3. Dec. 2023]. Dec. 2023. URL: https://www.sciencedirect.com/referencework/9780444527455/encyclopedia-of-electrochemical-power-sources.

[53] Eli Espinoza et al. "Practical Aspects of Cyclic Voltammetry: How to Estimate Reduction Potentials When Irreversibility Prevails". In: *J. Electrochem. Soc.* 166 (Jan. 2019), H3175–H3187. DOI: 10.1149/2.0241905jes.

[54] Jethrine H. Mugumya et al. "Synthesis and Theoretical Modeling of Suitable Co-precipitation Conditions for Producing NMC111 Cathode Material for Lithium-Ion Batteries". In: *Energy Fuels* 36.19 (Oct. 2022), pp. 12261–12270. ISSN: 0887-0624. DOI: 10.1021/acs.energyfuels.2c01805.

[55] Yiming Xu et al. "Online Soft Short-Circuit Diagnosis of Electric Vehicle Li-Ion Batteries Based on Constant Voltage Charging Current". In: *IEEE Trans. Transp. Electrif.* 9.2 (Sept. 2022), pp. 2618–2627. DOI: 10.1109/TTE.2022.3208066.

[56] Nutthaphon Phattharasupakun et al. "Effect of charging protocols on electrochemical performance and failure mechanism of commercial level Ni-rich NMC811 thick electrode". In: *Electrochem. Commun.* 139 (June 2022), p. 107309. ISSN: 1388-2481. DOI: 10.1016/j.elecom.2022.107309.

[57] Krishnarajsinh Jadav. "Design a Residential PV Power System with Battery Energy Storage". In: *International Journal on Advances in Engineering Technology and Science* 1 (Dec. 2015). URL: https://www.researchgate.net/publication/319329845_Design_a_Residential_PV_Power_System_with_Battery_Energy_Storage.

[58] Laurence A. Middlemiss et al. "Characterisation of batteries by electrochemical impedance spectroscopy". In: *Energy Rep.* 6 (May 2020), pp. 232–241. ISSN: 2352-4847. DOI: 10.1016/j.egyr.2020.03.029.

[59] Qihao Lin et al. “Electrochemical Impedance Spectroscopy (EIS) Explanation of Single Crystal Cu(100)/Cu(111) in Different Corrosion Stages”. In: *Materials* 16.4 (Feb. 2023), p. 1740. ISSN: 1996-1944. DOI: 10.3390/ma16041740.

[60] Lizhi Wen et al. “Effect of composite conductive agent on internal resistance and performance of lithium iron phosphate batteries”. In: *Ionics* 28 (July 2022). DOI: 10.1007/s11581-022-04491-w.

[61] Cengiz Temiz and Cengiz Temiz. “Scanning Electron Microscopy”. In: *Electron Microscopy*. IntechOpen, Apr. 2022. ISBN: 978-1-80355-946-9. DOI: 10.5772/intechopen.103956.

[62] Mukesh Kumar Singh and Annika Singh. “Chapter 17 - Scanning electron microscope”. In: *Characterization of Polymers and Fibres*. Buckingham, England, UK: Woodhead Publishing, Jan. 2022, pp. 387–419. ISBN: 978-0-12-823986-5. DOI: 10.1016/B978-0-12-823986-5.00008-7.

[63] Zhou Wang et al. “SOC evaluation of lithium batteries based on VKF, ampere-hour integration and unsteady open circuit voltage fusion method”. In: *2022 15th International Symposium on Computational Intelligence and Design (ISCID)*. IEEE, pp. 17–18. DOI: 10.1109/ISCID56505.2022.00057.

APPENDICES

.1 Three electrode setup

The three electrode setup was created in order to investigate anode and cathode overpotential contributions to discern what could be learned in relation to mass transport and rate capacity retention. In order to do this a stable reference electrode was tested as shown in the experimental method section. Figure .1.1 shows the stability of a gold wire reference electrode (GWRE) after the GWRE was lithiated for 2 hours using a current of 5 μA between the GWRE and a lithium metal electrode which was used as the working electrode.

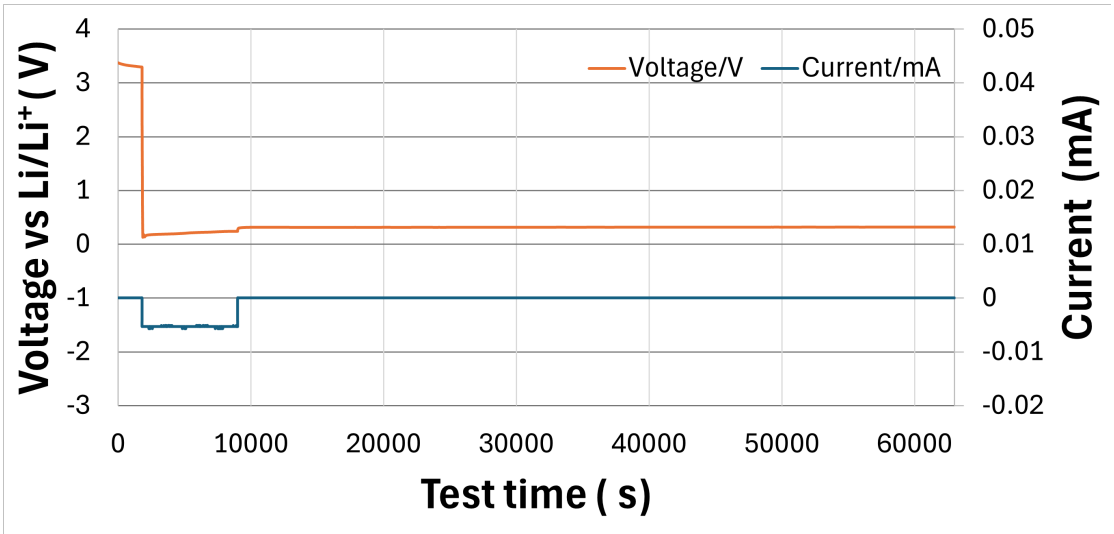

Figure .1.1: Figure shows the stable lithiation process for a lithium anode used as the working electrode and the reference electrode used as the other one.

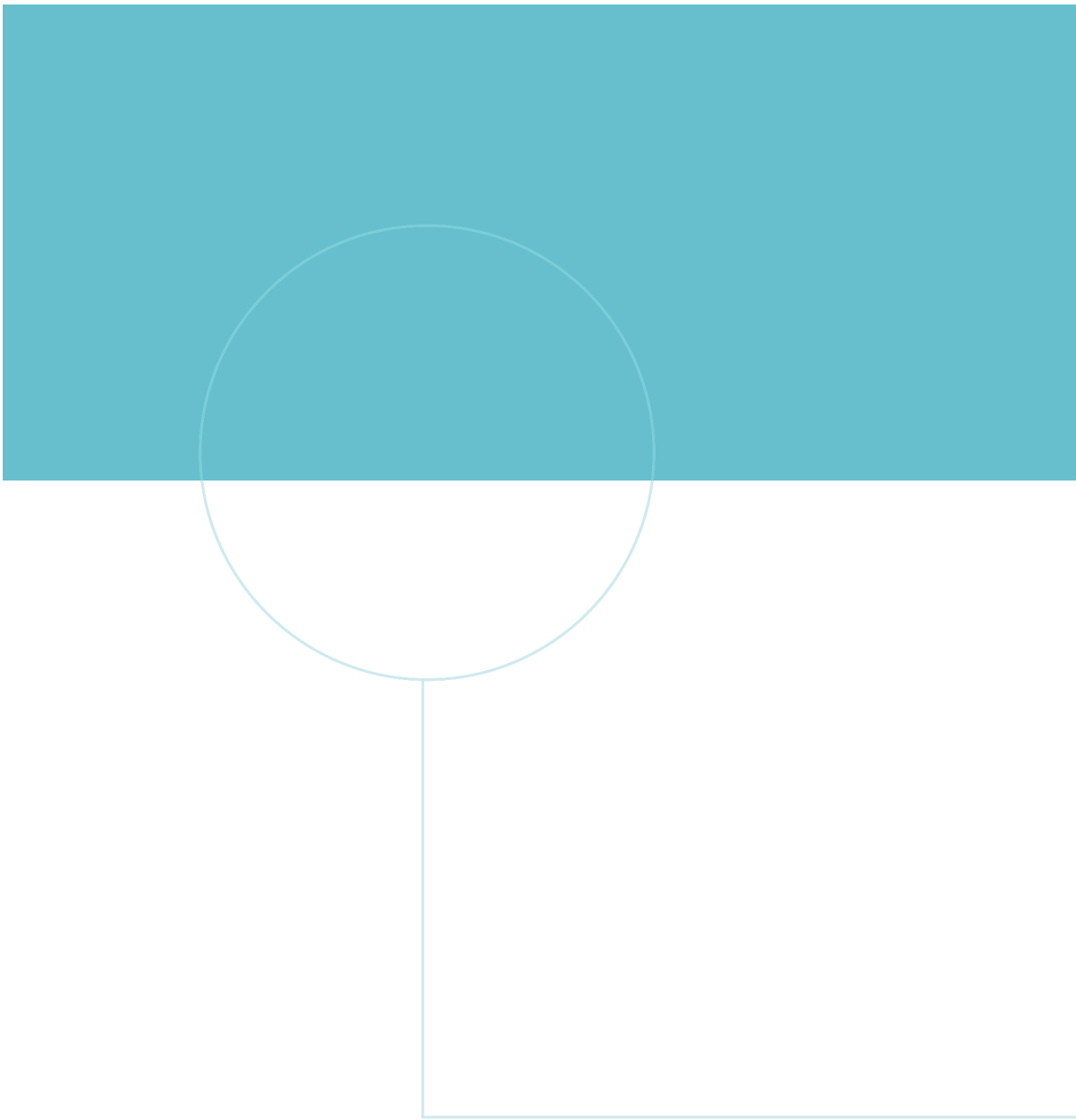

NTNU

Norwegian University of
Science and Technology